



# รายงานวิจัยฉบับสมบูรณ์

โครงการการสังเคราะห์และปรับแต่ง mesoporous LTA zeolite เพื่อ เพิ่มความสามารถในการดูดซับคาร์บอนไดออกไซด์ด้วย โลหะออกไซด์และกลุ่มเอมีน

โดย อ.ดร.กิ่งแก้ว ฉายากุล ชนาภัทรภณ และคณะ

เมษายน 2561

# สัญญาเลขที่ MRG5980081

# รายงานวิจัยฉบับสมบูรณ์

โครงการการสังเคราะห์และปรับแต่ง mesoporous LTA zeolite เพื่อ เพิ่มความสามารถในการดูดซับคาร์บอนไดออกไซด์ด้วย โลหะออกไซด์และกลุ่มเอมีน

ผู้วิจัย

สังกัด

อ.ดร.กิ่งแก้ว ฉายากุล ชนาภัทรภณ มหาวิทยาลัยขอนแก่น
 ศ.ดร.สุจิตรา ยังมี มหาวิทยาลัยขอนแก่น

สนับสนุนโดยสำนักงานกองทุนสนับสนุนการวิจัยและ มหาวิทยาลัยขอนแก่น

(ความเห็นในรายงานนี้เป็นของผู้วิจัย สกว.และต้นสังกัดไม่จำเป็นต้องเห็นด้วยเสมอไป)

# บทคัดย่อ

รหัสโครงการ: MRG5980081

ชื่อโครงการ : การสังเคราะห์และปรับแต่ง mesoporous LTA zeolite เพื่อเพิ่มความสามารถในการดูด

ซับคาร์บอนไดออกไซด์ด้วยโลหะออกไซด์และกลุ่มเอมีน

ชื่อนักวิจัย: ดร.กิ่งแก้ว ฉายากุล ชนาภัทรภณ

E-mail Address: kingkaew@kku.ac.th

ระยะเวลาโครงการ : 2 พฤษภาคม 2559 – 1 พฤษภาคม 2561

งานวิจัยนี้ศึกษาการสังเคราะห์และปรับแต่งสารดูดซับเพื่อเพิ่มความสามารถในการดูดซับ คาร์บอนไดออกไซด์ รวมทั้งศึกษาพฤติกรรมการดูดซับของคาร์บอนไดออกไซด์บนพื้นผิวของสารดูดซับ งานนี้แบ่งออกเป็น 2 ส่วน ส่วนแรกเน้นไปที่การสังเคราะห์และปรับแต่งซีโอไลต์เพื่อเพิ่มความสามารถ ในการดูดซับคาร์บอนไดออกไซด์ โดยเตรียมซีโอไลต์ด้วยวิธี sol-gel ด้วยสารละลายโซเดียมซิลิเกตและ อะลูมิเนียมไฮดรอกไซด์ ผลจากการดูดซับคาร์บอนไดออกไซด์พบว่าซีโอไลต์ที่เตรียมด้วยการเติม CTAB และ heptane มีปริมาณการดูดซับคาร์บอนไดออกไซด์ได้สูงกว่าเนื่องจากมีพื้นที่ผิวและปริมาตรรู พรุนที่สูง ซึ่งผลของการเติม CTAB และ heptane และกลไกการเกิดซีโอไลต์ได้ถูกเสนอ คือ ไมเซลล์ ของ CTAB และไอออนโซเดียมสามารถเกิดอันตรกิริยากับ aluminosilicate anion ได้มากขึ้น และส่งผล ให้อัตราการเกิดนิวคลีเอชันสูงขึ้น จึงทำให้ขนาดของผลึกซีโอไลต์เล็กลง ส่วนการเติม heptane ร่วมด้วย จะทำให้ไมเซลล์ของ CTAB มีความเป็นบวกมากขึ้นและส่งผลให้อันตรกิริยาระหว่าง aluminosilicate กับไมเซลล์มีมากขึ้น สำหรับงานในส่วนที่สองเป็นการศึกษาพฤติกรรมการดูดซับ คาร์บอนไดออกไซด์บน iron oxide ที่เติมลงบน MCM-41 โดยอาศัยเทคนิค in-situ CO<sub>2</sub> adsorption และติดตามด้วยเทคนิค X-ray absorption near edge structure (XANES) โดย iron oxide เตรียมด้วย ีวิธีเอิบชุ่มที่ความเข้มข้น 0.10, 0.25, 0.50, 0.75 และ 1.0 wt% ผลจากการดูดซับคาร์บอนไดออกไซด์ พบว่าการเติมโลหะออกไซด์ทำให้ความสามารถในการดูดซับเพิ่มขึ้นและ 0.50 wt%Fe/MCM-41 เป็น สารดูดซับที่ให้ปริมาณการดูดซับสูงสุด ทำการศึกษาอันตรกิริยาระหว่างคาร์บอนไดออกไซด์และอะตอม เหล็กด้วยเทคนิค XANES พบว่ามีการถ่ายโอน d-electron บางส่วนจากเหล็กไปที่ π\*-antibonding orbital ของคาร์บอนไดออกไซด์จึงทำให้การดูดซับเกิดได้มากขึ้น ซึ่งการดูดซับที่แข็งแรงมากขึ้นสามารถ แสดงให้เห็นได้ด้วยการเพิ่มขึ้นของค่าความร้อนของการดูดซับ

**คำสำคัญ**: การดูดซับคาร์บอนไดออกไซด์, ซีโอไลต์, CTAB และ heptane, In-situ CO<sub>2</sub> adsorption,

MCM-41

# **Abstract**

Project Code: MRG5980081

Project Title: The synthesis and modification of mesoporous LTA zeolite for enhancing CO2

adsorption by metal oxides and amine groups.

Investigator: Dr. Kingkaew Chayakul Chanapattharapol

E-mail Address: kingkaew@kku.ac.th

Project Period: 2<sup>nd</sup> May 2016- 1<sup>st</sup> May 2018

In this work, synthesis and modify of adsorbent for enhancing CO2 adsorption capacity were investigated. Moreover, the CO2 adsorption behavior on synthesized adsorbents was also studied. This project is divided into 2 parts. The first part was focusing on synthesis and modify the surface properties of zeolite by addition of cetyltrimethylammonium bromide (CTAB) and heptane for enhancing CO2 uptake. The zeolite was prepared from a sodium silicate solution and Al(OH)<sub>3</sub> by sol-gel method. The CO<sub>2</sub> adsorption capacity of the synthesized zeolite with the addition of CTAB and heptane increased which was due to the higher surface area and pore volume. The role of CATB and heptane on zeolite formation mechanism was proposed. Interaction between CTAB micelles and sodium cations with aluminosilicate anions led to an increase in the nucleation rate and smaller crystalline sizes. The addition of heptane resulted in higher positively charged CTAB micelles and improved the affinity between the micelles and aluminosilicate anions. The second part was CO2 adsorption study on iron oxide doped MCM-41 by using in-situ CO<sub>2</sub> adsorption investigated by X-ray absorption near edge structure (XANES). The iron oxide doped on MCM-41 samples were prepared by impregnation method with iron concentrations of 0.10, 0.25, 0.50, 0.75 and 1.0 wt%. Adsorption isotherm indicated that modifying MCM-41 with iron oxide can increase CO<sub>2</sub> adsorption with the best result being achieved with 0.50 wt%Fe/MCM-41. Interaction between CO<sub>2</sub> and Fe atoms were studied by Xray absorption near edge structure (XANES). XANES spectra indicated the transfer of metal delectrons to CO<sub>2</sub> π\*-antibonding orbital giving rise to additional adsorption. Stronger bonding between CO2 and the adsorbent was indicated by the increase of the isosteric heat of adsorption.

**Keywords**: CO<sub>2</sub> adsorption, Zeolite, CTAB and heptane, Iron oxide, In-situ CO<sub>2</sub> adsorption, MCM-41

# สัญญาเลขที่ MRG5980081

# โครงการการสังเคราะห์และปรับแต่ง mesoporous LTA zeolite เพื่อเพิ่มความสามารถในการ ดูดซับคาร์บอนไดออกไซด์ด้วยโลหะออกไซด์และกลุ่มเอมีน

(The synthesis and modification of mesoporous LTA zeolite for enhancing CO<sub>2</sub> adsorption by metal oxides and amine groups)

# **Executive Summary**

Global warming resulting from the emission of greenhouse gases, especially CO<sub>2</sub>, has become a widespread concern in recent years. The concentration of atmospheric CO<sub>2</sub> is increasing rapidly. Anthropogenic CO<sub>2</sub> is emitted primarily from fuel combustion and human activities. There is an urgent need for the development of technology to reduce the CO<sub>2</sub> emissions from anthropogenic sources. Several methods have been used to reduce and remove the CO<sub>2</sub> such as liquid amine absorption, solid adsorbents, cryogenic technique and selective membrane. Among these methods, the adsorption technology is considered to be more convenient, energy-efficient and able to overcome the drawbacks of the traditional liquid amine absorption process, including solvent degradation and equipment corrosion. Many different porous materials have been used as CO<sub>2</sub> adsorbents such as zeolite, carbon, silica and metal-organic frameworks. Among these, zeolites are widely used as an adsorbent for gas adsorption. Zeolites are crystalline aluminosilicates compounds which have specific physicochemical properties for extensive applications such as high thermostability, high ion exchange, high selectivity, reversibility for hydration and dehydration, high surface area and large vacant sites. Thus, zeolites have been widely studied as adsorbents for CO<sub>2</sub> capture.

The aim of this work was to synthesis of mesoporous LTA zeolite by using organosilane surfactants to expand the micropore to mesopore structure. The larger cavities inside the mesoporous LTA zeolite will be available for impregnation by basicity functional groups for enhancing  $CO_2$  adsorption properties. Unfortunately, expanding the pore structure of zeolite NaA by using cationic surfactant (cetyltrimethylammonium bromide; CTAB) was not successful. However, on the synthesis period, we found that zeolite NaX was formed during synthesized of zeolite NaA and its  $CO_2$  adsorption performance was higher than that of zeolite NaA. Therefore, we further worked on synthesis of zeolite NaX and modified the surface properties by addition of CATB and hydrocarbon to enhance  $CO_2$  adsorption capacity.

After we have changed the plan, we have divided this work into two parts. The first part was synthesis of zeolite NaX and modify its surface properties (surface area, pore size, pore volume and morphology) to enhance CO<sub>2</sub> adsorption ability. In this part, Zeolites X were successfully synthesized by gelation with a sodium silicate solution and Al(OH)3 as silicon and aluminuim sources. All samples were characterized by XRD, SEM and N2 adsorptiondesorption techniques. The synthesized zeolites exhibited a characteristic of zeolite type X with octahedral crystal. The effects of the addition of additives (CTAB and heptane) and aging time on surface properties, morphology and CO<sub>2</sub> adsorption performance were investigated. The addition of CTAB and heptane increased zeolite crystallinity by affecting the nucleation process. The surface area and pore volume of zeolite products were increased due to smaller crystalline size. These results can be explained to be effected by the increase in the nucleation rate of zeolite caused by the added substances. Moreover, then number of crystallinities of zeolite were increased with the increase of aging times. Due to higher surface area and pore volume upon CTAB and heptane addition, the CO2 adsorption capacities of the synthesized zeolite X increased significantly. The study indicated that an aging time of 7 days is needed for completing the crystallization process.

The second part was focus on CO<sub>2</sub> adsorption behavior on metal oxide doped on MCM-41. Since basic metal oxide was favor to interact with acidic CO<sub>2</sub> molecule and resulted in enhancing CO<sub>2</sub> uptake. Therefore, in this part, iron oxide doped MCM-41 was used to study CO<sub>2</sub> adsorption by in-situ CO<sub>2</sub> adsorption which monitored by time-resolved X-ray absorption spectroscopy and the CO<sub>2</sub> adsorption behavior was discussed. CO<sub>2</sub> adsorption of iron oxide doped on mesoporous MCM-41 was studied and the results showed that the CO<sub>2</sub> adsorption capacity of 0.50 wt%Fe/MCM-41 was higher than that of the undoped MCM-41. The characteristic results from XRD, N<sub>2</sub> adsorptiondesorption and SEM revealed that the mesoporous structure and morphology of iron oxide doped MCM-41 were not different from the starting mesoporous material. The isosteric heat of adsorption indicated that the interaction between CO<sub>2</sub> and iron oxide doped MCM-41 was physical adsorption. The enhanced CO<sub>2</sub> adsorption of iron oxide doped MCM-41 was attributed partly to the increase of surface area and partly to electron transfer from metal d-orbital to CO<sub>2</sub> antibonding 2πu. This experiment

gave an insight to the techniques that may be used to improve  ${\rm CO_2}$  adsorption upon the modified adsorbate.

Output: The research outcome included two international publication papers

- Somkiat Krachuamram, Chanaiporn Danvirutai, Sujittra Youngme, <u>Kingkaew Chayakul Chanapattharapol\*</u>, Effects of Cetyltrimethylammonium Bromide and Heptane on the Surface Properties and CO<sub>2</sub> Adsorption of Zeolite NaX, *Journal of the Chinese Chemical Society* 64 (2017) 658-665.
- Kingkaew Chayakul Chanapattharapol\*, Somkiat Krachuamram, Sujittra Youngme, Study of CO<sub>2</sub> adsorption on iron oxide doped MCM-41, *Microporous and Mesoporous Materials* 245 (2017) 8-15.

# **TABLE OF CONTENTS**

ABSTRAC <sup>*</sup>	Γ (IN THAI)	I
ABSTRAC <sup>*</sup>	T (IN ENGLISH)	II
EXECUTIV	E SUMMARY	III
PART 1	EFFECT OF CETYTRIMETHYLAMMONIUM BROMIDE AND	1
	HEPTANE ON THE SURFACE PROPERTIES AND CO <sub>2</sub>	
	ADSORPTION OF ZEOLITE NaX	
	Introduction	1
	Experimental	2
	Results and Discussion	3
	Conclusions	14
PART 2	STUDY OF CO <sub>2</sub> ADSORPTION ON IRON OXIDE DOPED MCM-41	17
	Introduction	17
	Experimental	19
	Results and Discussion	21
	Conclusions	35
OUTPUT O	F THE RESEARCH	38
APPENDIC	ES	40

#### PART 1

# PROPERTIES AND CO<sub>2</sub> ADSORPTION OF ZEOLITE NaX

# 1. INTRODUCTION

The emission of carbon dioxide to the atmosphere has been identified as a major contributor to climate change. Since the beginning of the industrial age in ca. 1800, the concentration of CO<sub>2</sub> in the atmosphere has rapidly increased and it is widely accepted that carbon capture and storage will play a crucial role in the reduction of greenhouse gases. Current CO<sub>2</sub> capture technologies include absorption, adsorption and selective membrane [1-3]. Among these technologies, adsorption is considered to be the most convenient and energy-efficient.

Zeolites are widely used for CO<sub>2</sub> adsorption due to their well-defined porous structure. As a result, the question of how to enhance CO<sub>2</sub> uptake is now an interesting topics. The way to enhance adsorption capacity is to modify the surface properties of adsorbents such as by changing crystalline size and morphology. It has been reported that increases in surface area can lead to increases in CO2 adsorption sites [4]. Increasing the surface area of adsorbents can be done by reducing crystalline sizes. The crystal size of zeolite is controlled by the rate of nucleation and crystal growth. It is known that both rates decrease with a lowering of temperature [5, 6]. Lower nucleation rates give rise to larger crystalline sizes. However, the growth rate varies more strongly with temperature than the nucleation rate. As the temperature decreases, the decrease in the nucleation rate is less significant and the growth rate predominately decreases leading to smaller crystalline sizes [7]. Moreover, aging the synthesis mixture before crystallization is also usually used to control the size of zeolite crystals. The nucleation rate is significant at room temperature while the growth rate is negligible [8]. Therefore, aging at low temperature may allow for increase in the number of nuclei or nuclei precursors which will lead to smaller zeolite crystals. It has been reported that the surface properties of zeolite can be modify by using the coaddition of surfactant and organic additives [9, 10]. F. G. Gu and coworkers [11] reported a new strategy to synthesis of hierarchical mesopore zeolite by CTAB with cosolvents (tertbutyl alcohol and 1,3,5-trimethylbenzene) and

tested for their adsorptive performance for *N*-nitrosopyrrolidine. Some research groups have tried to synthesize a smaller crystalline size by adding surfactants such as CTAB and TMAOH [12, 13]. CTAB is cationic surfactant that is widely used as a template in synthesis of porous materials and some works have reported that CTAB was an additive substance to increase the nucleation rate which led to smaller crystalline size. Therefore, in this work, zeolite X was synthesized by gelation method. The effects of adding CTAB and heptane on surface properties, morphologies and CO<sub>2</sub> adsorption were investigated.

#### 2. EXPERIMENTAL

#### 2.1 Synthesis of zeolite adsorbent

Zeolite X was synthesized by gelation. Sodium silicate solution and aluminium hydroxide were used as silicon and aluminium sources, respectively. For zeolite synthesis, sodium aluminate was prepared by dissolving 2.72 g of sodium hydroxide in deionized water (40 mL) and then 2.79 g of aluminium hydroxide was added and stirred at room temperature for 4 h. The prepared sodium aluminate was mixed with a sodium silicate solution under stirring. The mixture was stored in polypropylene bottle and aged at room temperature for 1, 3 and 7 days in order to study the effects of aging time. The obtained mixture was then heated in an oven at 372 K for 4 h. The product was filtered, washed by ethanol, followed by water and dried at 343 K for 12 h and then calcined at 823 K for 4 h. The final products were denoted as Z\_xD, where x was aging time.

To study the effects of additive substances, the preparation procedure was similar to the above process in which CTAB and heptane were added after sodium silicate and sodium aluminate were mixed. The final products were labeled as ZC\_xD for CTAB addition samples and ZCH xD for CTAB and heptane coaddition.

### 2.2 Standard Characterization techniques

X-ray diffraction (XRD) patterns were obtained by a PANalytical Empyrean X-ray diffractometer with Cu K $_{\infty}$  radiation ( $\lambda$  = 1.5406 Å). XRD patterns were used to confirm the structure of the prepared zeolite by comparing with the standard zeolite NaX database. The diffraction patterns were obtained in the  $2\theta$  range of  $5^{\circ}$  to  $50^{\circ}$ .

The BET surface area, pore volume and average pore size were obtained from  $N_2$  adsorption-desorption isotherm at 77 K and investigated on an Autosorb-1 Quantachrome instrument. The samples were degassed at 423 K for 4 h before the adsorption experiment. The BET surface area was calculated by using the multipoint-BET method in the relative pressure  $(P/P_o)$  range of 0.05 to 0.30. The micropore volume was calculated by using the statistical thickness method in the relative pressure  $(P/P_o)$  range of 0.20 to 0.40. The pore volume was evaluated at a  $P/P_o \sim 1$ . Pore size distribution was calculated by NLDFT method.

The morphologies of synthesized zeolites were investigated by using a LEO 1450VP Scanning Electron Microscope (SEM) instrument. Before the scanning process, the samples were prepared by dispersing the grain powder on carbon tape that attached on the specimen stub. Then, the samples were coated with gold to reduce the electron charge.

# 2.3 CO, adsorption

 ${
m CO_2}$  adsorptions of all synthesized adsorbents were performed on a NOVA 1200 e instrument (Quantachrome) at the desired temperature. About 200 mg of samples were outgassed at 300  $^{\circ}{\rm C}$  for 3 hours in vacuum prior to adsorption measurement.

# 3. RESULTS AND DISCUSSION

# 3.1 Aging time

Table 1 displays the summary of synthesis conditions of all samples. The added amounts of CTAB (0.070 mol/dm³) and heptane (0.085 mol/dm³) were kept constant. The mole ratio of the synthesized zeolite was 5.00Na<sub>2</sub>O: 1.00Al<sub>2</sub>O<sub>3</sub>: 3.00SiO<sub>2</sub>: 138.00H<sub>2</sub>O: 0.16CTAB: 0.19 heptane. Figure 1 illustrates the XRD patterns of all samples with and without CTAB and heptane. In the case of zeolite without CTAB and heptane (Z\_xD), the zeolite X cannot be formed in less than 7 days. Upon the introduction of CTAB (ZC\_xD), the zeolite X was formed within 3 days, however, existent of zeolite NaA having less complex secondary building units (D4R) was also detected. The impurity NaA phase disappeared when the aging time increased to 7 days. In the coaddition of CTAB and heptane (ZCH\_xD), the zeolite NaX can be formed within 1 day with some zeolite NaA impurity. These NaA impurity peaks are reduced with an increase of aging time and disappear after 7 days aging. The XRD results illustrate the increasing characteristic peak intensities with increasing aging time. However, the increasing

the aging time up to 14 days shows a nonsignificant improvement in intensities from that of the 7 day case. It can be concluded that the crystallinity of synthesized samples increases with the aging time and crystallization is completed within 7 days. This is in agreement with several works [14, 15]. Upon the addition of CTAB and heptane, the time for formation of zeolite was lowered. Therefore, it can be concluded that the addition of CTAB and heptane enhanced the nucleation process. However, sufficient aging time is required to produce good crystallinity.

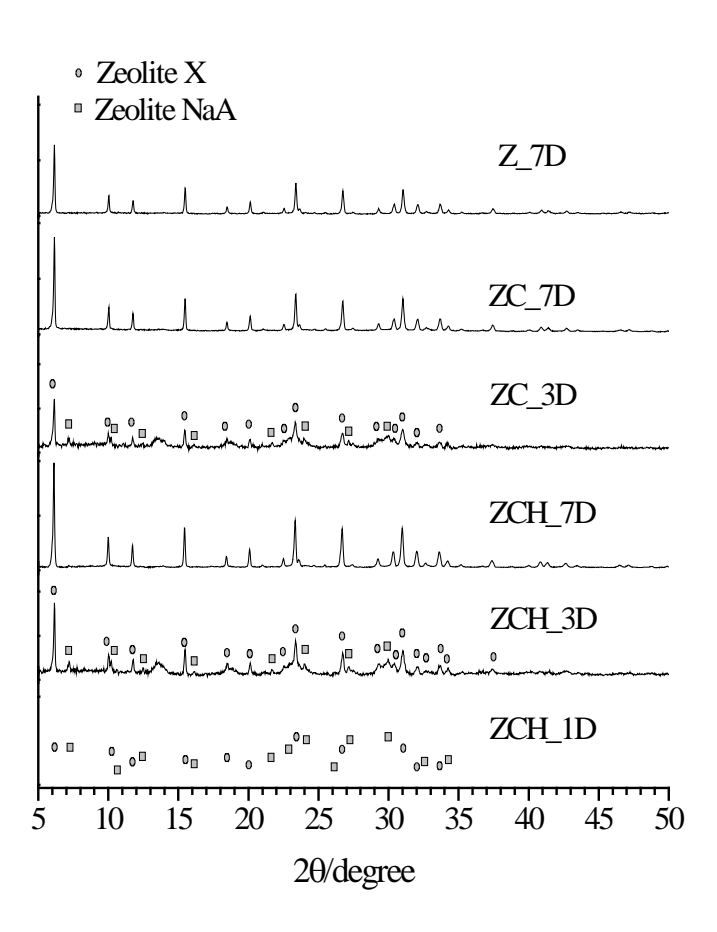
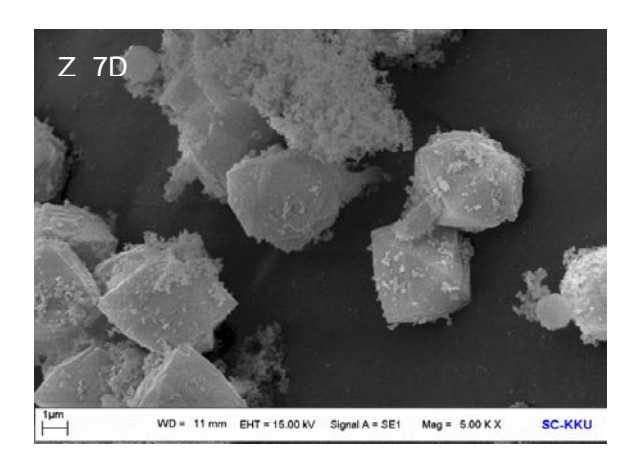


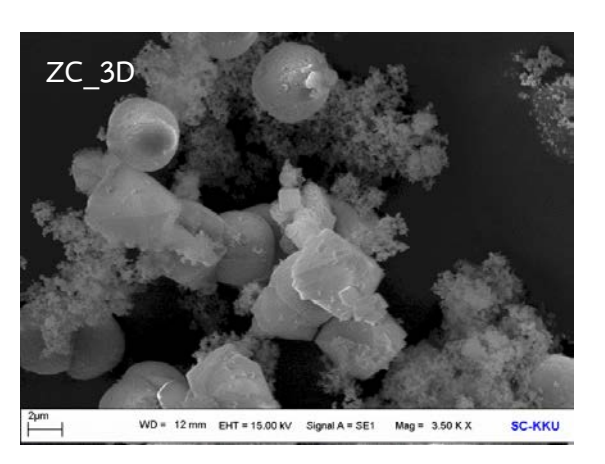
Figure 1 XRD patterns of Z\_7D, ZC\_3D, ZC\_7D, ZCH\_1D, ZCH\_3D and ZCH\_7D.

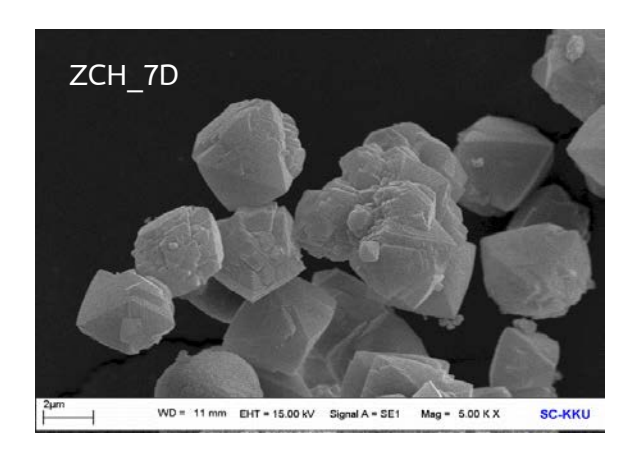
Table 1 The synthesis condition of all samples.

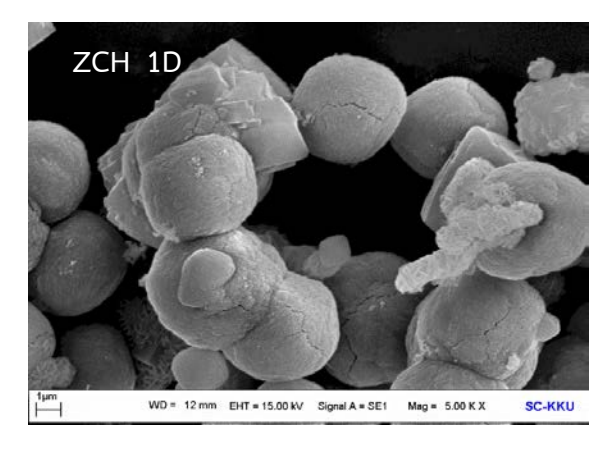
Sample code	Si source	Al source	CTAB (mol/dm <sup>3</sup> )	Heptane (mol/dm <sup>3</sup> )	Crystallization time (days)
Z_7D	Na <sub>2</sub> SiO <sub>3</sub> (I)	Al(OH) <sub>3</sub>	-	-	7
ZC_3D	Na <sub>2</sub> SiO <sub>3</sub> (I)	AI(OH) <sub>3</sub>	0.070	-	3
ZC_7D	Na <sub>2</sub> SiO <sub>3</sub> (I)	AI(OH) <sub>3</sub>	0.070	-	7
ZCH_1D	Na <sub>2</sub> SiO <sub>3</sub> (I)	AI(OH) <sub>3</sub>	0.070	0.085	1
ZCH_3D	Na <sub>2</sub> SiO <sub>3</sub> (I)	AI(OH) <sub>3</sub>	0.070	0.085	3
ZCH_7D	Na <sub>2</sub> SiO <sub>3</sub> (I)	AI(OH) <sub>3</sub>	0.070	0.085	7

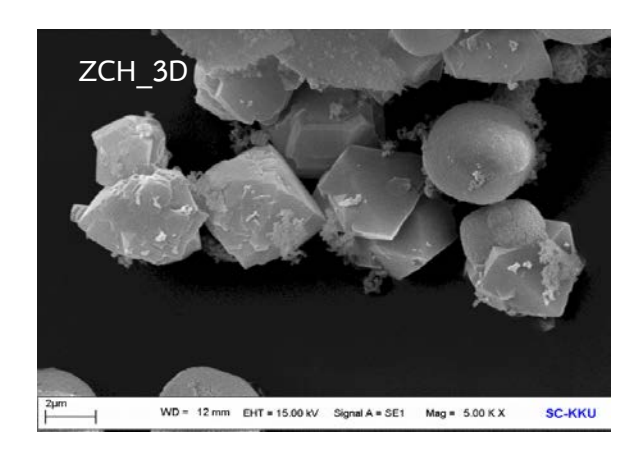
SEM micrographs of all samples are shown in Figure 2. In the absence of CTAB and heptane (Z\_7D), octahedral crystal with many impurities was found. For the sample with CTAB (ZC\_xD), some cubic-like structures were found to coexist with octahedral crystal of zeolite NaX at a crystallization time of 3 days. The crystalline size was 4-5 μm and it was clearly visible that the crystalline size was not uniform. The cubic-like structure disappeared when the crystallization time was increased to 7 days and crystalline size was more uniform (4-5 μm). For the coaddition of CTAB and heptane samples (ZCH\_1D, ZCH\_3D and ZCH\_7D), it was found that ZCH\_1D had mainly cubic-like crystal for the sample with 1 day aging time. The octahedral structure began to exist upon 3 days aging and become uniform after 7 days of aging. The crystalline sizes of all these samples decreased with increasing aging time, i.e. 4μm, 3.5μm and 3μm for ZCH\_1D, ZCH\_3D and ZCH\_7D, respectively. The results from SEM micrographs agree with the XRD patterns that lower crystallinity of zeolite NaX was due to impurities phases of zeolite NaA. Upon prolonging aging time, higher crystallinity was observed by the presence of pure octahedral crystal of zeolite NaX.











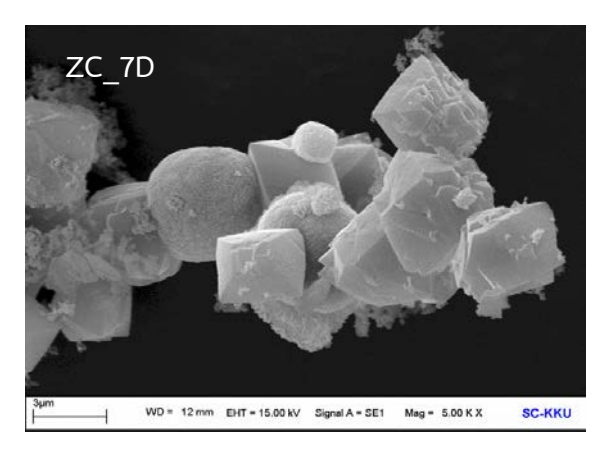
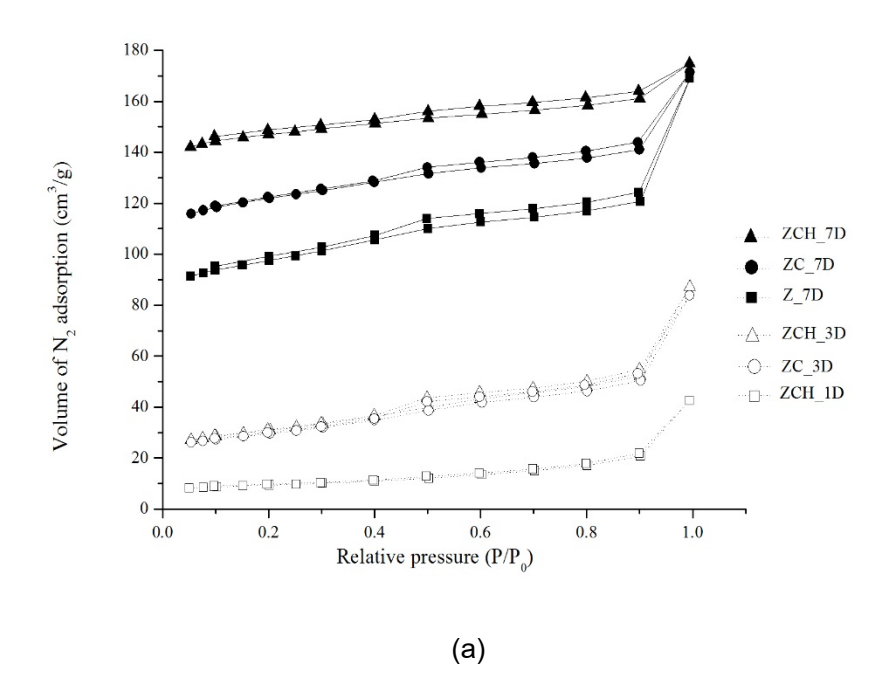


Figure 2 SEM micrographs of Z\_7D, ZC\_3D, ZC\_7D, ZCH\_1D, ZCH\_3D and ZCH\_7D.

# 3.2 Surface properties

The N<sub>2</sub> adsorption-desorption isotherms of the synthesized samples are shown in Figure 3(a). All samples exhibited a hysteresis loop which indicated the existence of porous material. The addition of CTAB and heptane led to two groups of products. For low aging times, the products (ZC\_3D, ZCH\_3D and ZCH\_1D) showed lower N<sub>2</sub> adsorption amounts which was due to impurities of zeolite NaA. For longer aging times, the products (Z\_7D, ZC\_7D and ZCH\_7D) showed higher N<sub>2</sub> adsorption. Figure 3(b) illustrates the pore size distribution of all samples. It was found that pore size distribution was almost unchanged upon the addition of CTAB and heptane. The surface properties of the synthesized samples are summarized in Table 2. The total surface area is the summation of external surface area and internal surface area (micropore surface area). For 7 days aging time, the micropore surface area was higher than external surface area, which indicated the microporous structure. The total surface area of samples were increased with the addition of CTAB and heptane. The sample without CTAB and heptane (Z\_7D) exhibited low surface area and pore volume. In contrast, when CTAB and heptane were added, the surface area and pore volume increased and this was due to smaller crystalline sizes.

It is clearly seen that samples with low aging times (1D and 3D) had very low internal surface areas as well as low pore volume. Together with the results from XRD and SEM this indicated the coexistence of zeolite NaA which is not  $N_2$ -adsorption favorable. This result indicates that lower aging time cannot bring up complete crystallization and that at least 7 days are needed for this to occur.



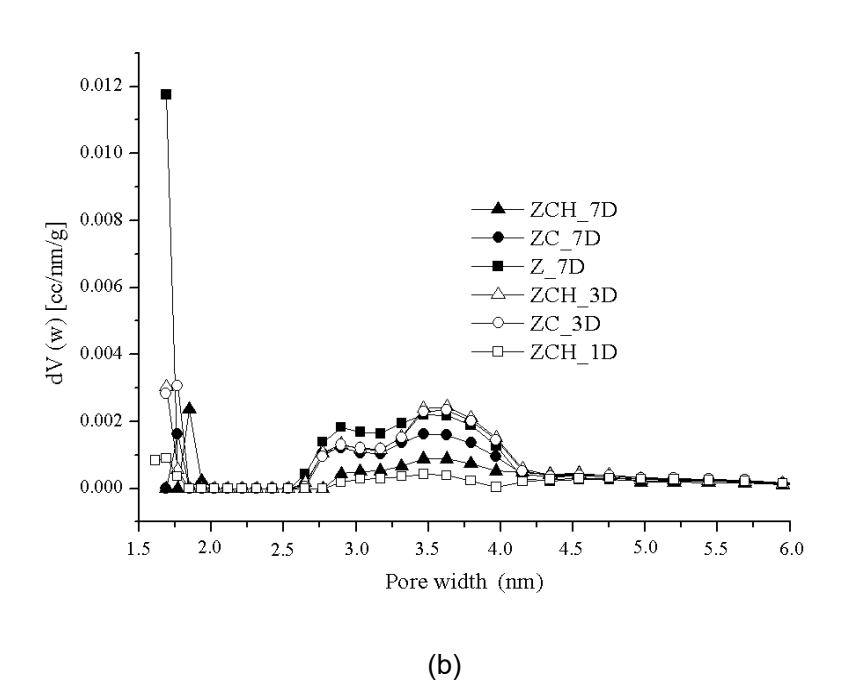


**Figure 3** (a) N<sub>2</sub> adsorption-desorption isotherms of Z\_7D, ZC\_3D, ZC\_7D, ZCH\_1D, ZCH\_3D and ZCH\_7D.

(b) Pore size distribution of Z\_7D, ZC\_3D, ZC\_7D, ZCH\_1D, ZCH\_3D and ZCH\_7D.

Table 2 Specific surface area, pore volume of all synthesized samples.

Camplas	Specific surface area (m²/g)			Pore volume (cm³/g)
Samples	Total	External	Internal	Pore volume (cm /g)
ZCH_1D	30.52	18.66	11.85	0.0600
ZC_3D	96.68	63.65	33.04	0.1300
ZCH_3D	100.8	64.51	36.33	0.1353
Z_7D	304.3	96.11	208.2	0.2620
ZC_7D	374.4	74.30	300.1	0.2658
ZCH_7D	447.8	49.97	397.8	0.2710

# 3.3 CO<sub>2</sub> adsorption properties

 ${
m CO_2}$  adsorption isotherms at 298 K of all synthesized samples are illustrated in Figure 4. ZCH\_7D shows the highest  ${
m CO_2}$  adsorption capacity of 3.00 mmol/g at P/P<sub>o</sub>~1. The addition of CTAB and heptane led to an increase in  ${
m CO_2}$  uptake, which was due to higher surface area and pore volume. Zeolite with shorter aging time showed decreased  ${
m CO_2}$  uptake due to the existence of zeolite NaA phase and incompleted crystallization which led to lower surface area and pore volume.

Figure 5 displays the plots of  $CO_2$  adsorption as a function of surface area and pore volume of synthesized zeolite. This points to a direct correlation between  $CO_2$  uptake and surface area and pore volume. XRD and SEM indicate the decreases in crystalline size of zeolite leading to increases of surface area and pore volume and consequently increases in  $CO_2$  adsorption.

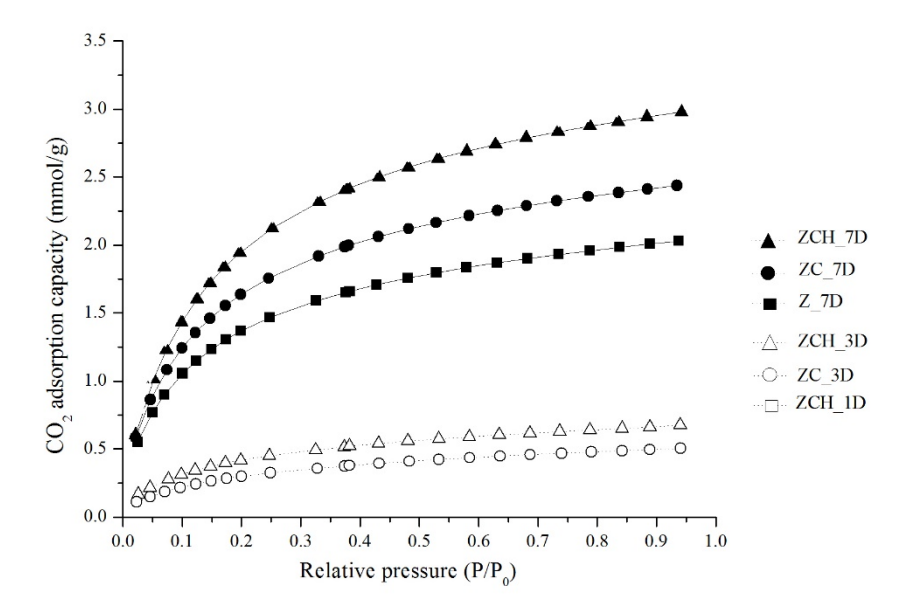
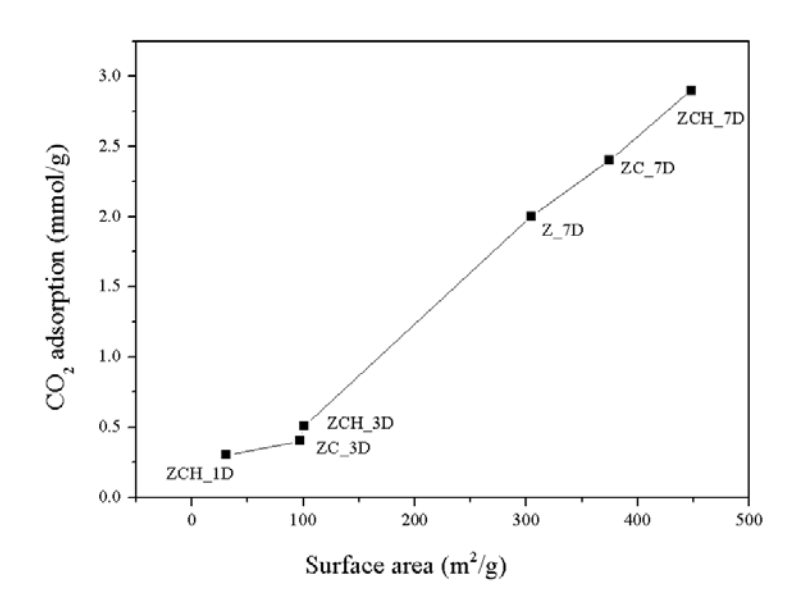
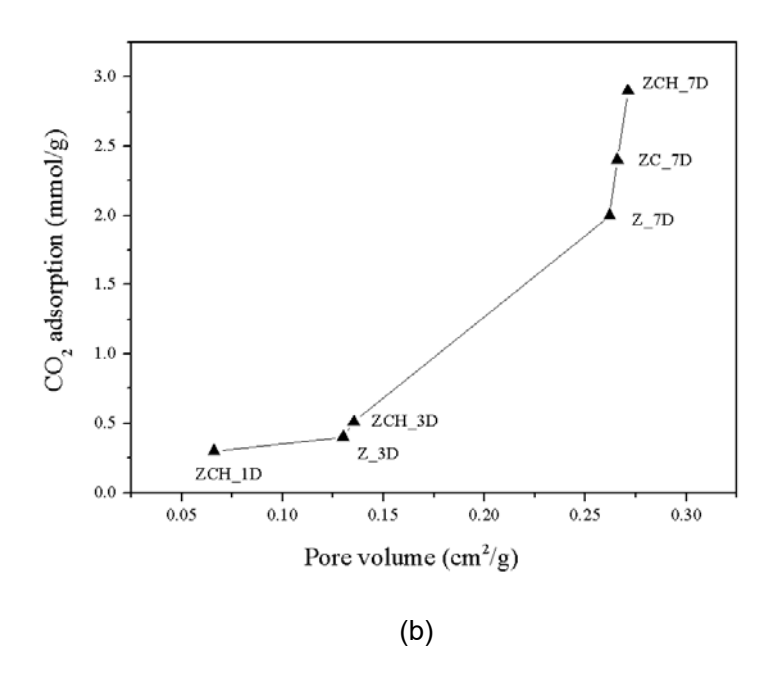


Figure 4  $\,{\rm CO}_2$  adsorption isotherm at 298 K of all synthesized samples.



(a)



**Figure 5** (a) The plots of CO<sub>2</sub> adsorption as a function of surface area and (b) pore volume of all synthesized samples.

# 3.4 Effect of CTAB and heptane

Zeolite formation mechanism requires two main processes: nucleation and crystallization. In order to modify its properties, these two processes must be perturbed. For nucleation, the temperature of synthesis condition can affect the nucleation process, i.e. room temperature aging can enhance the number of the nuclei and reduce crystal size [16]. The addition of some organic substances can speed up the nucleation process. For the crystallization process, a higher reaction temperature would lead to a higher crystallization rate [17, 18]. Zeolite formation mechanisms have been proposed and it can be summarized as follows [19];

- 1. Silicon and aluminium sources were solubilized in a basic medium (such as NaOH) to form an amorphous reactant which is called primary amorphous phase. This phase contains silicate and aluminate tetrahedral units.
- 2. Heating the mixture (above 100 °C) in an autoclave. Prior to this step, the mixture is usually left for aging at a period of times (hours to few days).
- 3. The formation of secondary amorphous phase with short range order. The secondary amorphous phase is a linkage of silicate and aluminate tetrahedral unit by sharing oxygen

atoms. This species is also called aluminosilicate anion and is proposed to be a nucleation precursor.

4. Growth of zeolite crystal when the nuclei reaches a critical size.

It is known that controlling the nucleation process can lead to a desired size of zeolite crystal. Nucleation is the rearrangement of reactant molecules into a cluster of product phase large enough to grow irreversibly to a macroscopic size. This cluster is defined as a nucleus or critical nuclei. Crystal growth is the incorporation of molecules at the surface of a crystal causing an increase in size [19]. It has been reported that cation in basic medium (Na<sup>+</sup>) and organic structure-directing agents plays a role in the nucleation process by surrounding themselves with aluminosilicate anion in preferred geometry according to electrostatic and van der Waals interaction [20, 21].

Figure 6 proposes the zeolite formation mechanism for this study. Pathway (a) illustrates a general nucleation process. Sodium cations are surrounded by water molecules and this hydration shell can be partially replaced by silicon and aluminium tetrahedral (oxygen of tetrahedral species replaces oxygen of water) to form secondary building units via condensation reaction.

The proposed mechanism for CTAB addition is displayed in pathway (b). CTAB is a cationic surfactant and can perturb the nucleation process. The aluminosilicate anion can rapidly form upon the addition of CTAB by more electrostatic interaction between aluminosilicate anion and hydrophilic part of CTAB micelles. The nucleation rate is increased by increases in the nuclei number resulting in smaller crystalline size.

The effect of coaddition of CTAB and heptane is illustrated in pathway (c). The influence of heptane can be described in terms of the swelling effect. Incorporating heptane molecules in the inner core of micelle will expand the size of micelle leading to a faster nucleation rate and smaller crystalline sizes. [22]. Kunieda et al. [23] studied the swelling effect of n-decane on the micelles of polyoxyethylenedodecyl ether. They explained the swelling effect by using the solubilization of heptane molecule in the core of the micelle. The solubilization of alkane can increase the packing parameter of surfactant aggregations [23]. The packing parameter in surfactant-aqueous system is expressed as

$$g = \frac{v_L}{\alpha_s l} \tag{1}$$

Where  $\, V_L \,$  is the total volume of lipophilic tails of surfactant plus the organic additives,  $\, C_s \,$  is the effective cross sectional area of the hydrophilic headgroups at the micelle-aqueous interface and I is the kinetic length of hydrophobic chain of surfactant [23]. Kunieda et al. [23] stated that swelling is the effect of oil to increase the volume of liphophilic part without changing the  $lpha_{
m s}$ value. From pore size distribution results, it was found that the addition of heptane did not lead to an increase in pore size. This means that the solubilization of heptane in the core of CTAB micelles increased  $V_{\text{L}}$  , which  $\,$  led to an increase in the packing parameter (g) of the surfactant micelles and made them more positive. Therefore, increasing the charge density of micelles together with increasing their volume probably led to an improvement in the affinity between the micelles and the aluminosilicate anions [14, 23]. This higher affinity led to a higher nucleation rate and higher nuclei number. This explanation can be evidenced by the results from XRD, SEM and particle analysis. From XRD patterns, it is clearly seen that zeolite can be formed with a shorter time upon the addition of CTAB. Moreover, the addition of heptane led to more rapidly formation of zeolite. Therefore, it can be concluded that addition of CTAB led to an increase in the nucleation rate by increasing the number of nuclei. From this effect, small crystal sizes were obtained resulting in higher pore volume and surface area.

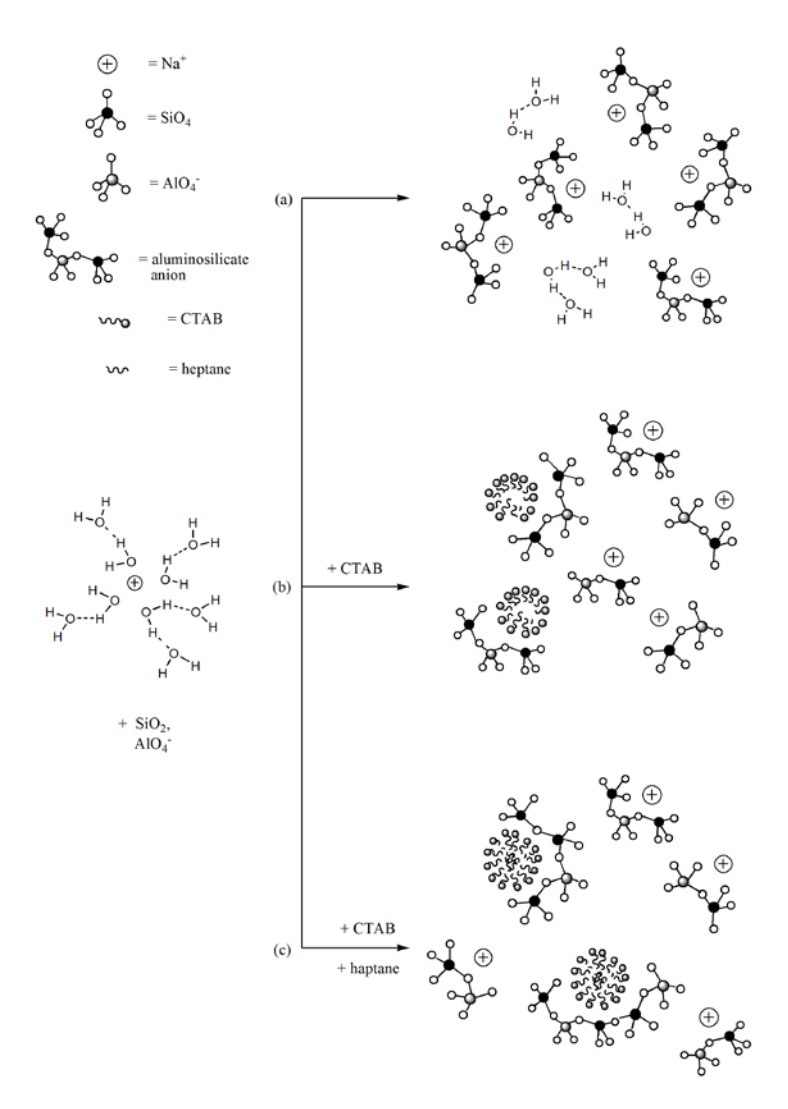


Figure 6 Proposed zeolite formation mechanism.

# 4. CONCLUSION

Zeolites X were successfully synthesized by gelation with a sodium silicate solution and Al(OH)<sub>3</sub> as silicon and aluminuim sources. All samples were characterized by XRD, SEM and N<sub>2</sub> adsorption-desorption techniques. The synthesized zeolites exhibited a characteristic of zeolite type X with octahedral crystal. The effects of the addition of additives (CTAB and heptane) and aging time on surface properties, morphology and CO<sub>2</sub> adsorption performance were investigated. The addition of CTAB and heptane increased zeolite crystallinity by affecting the nucleation process. The surface area and pore volume of zeolite products were increased due to smaller crystalline size. These results can be explained to be effected by the increase in the nucleation rate of zeolite caused by the added substances. Moreover, then number of

crystallinities of zeolite were increased with the increase of aging times. Due to higher surface area and pore volume upon CTAB and heptane addition, the CO<sub>2</sub> adsorption capacities of the synthesized zeolite X increased significantly. The study indicated that an aging time of 7 days is needed for completing the crystallization process.

#### **REFERENCES**

- 1. K.K. Pant Akanksha, V.K. Srivastava, Chem. Eng. J. 2007, 133, 229.
- 2. A. Anson, C.C.H. Lina, S.M. Kuznickia, J.A. Sawadab, Chem. Eng. Sci. 2009, 64, 3683.
- 3. A. Brunetti, F. Scura, G. Barbieri, E. Drioli, J. Membr. Sci. 2010, 359, 115.
- 4. A. Akgsornpeak, T.Witoon, T. Mungcharoen, J. Limtrakul, Chem. Eng. J. 2014, 237, 189.
- 5. N.N. Feoktistova, S.P. Zhdanov, W. Lutz, M. B.ulow, Zeolites 1989, 9, 136.
- 6. S. Mintova, V. Valtchev, E. Vultcheva, S. Veleva, Zeolites 1992, 12, 210.
- 7. H. J. Koroglu, A. Sarioglan, M. Tatlier, A. Erdem--Senatalar, O. T. Savascia, *J. Cryst. Growth* **2002**, 241, 481.
- 8. F. di Renzo, Catal. Today 1998, 41, 37.
- 9. W. Schwieger, A. G. Machoke, T. Weissenberger, A. Inayat, T. Selvam, M. Klumpp, A. Inayat, *Chem. Soc. Rev.*, **2016**, 45, 3353.
- 10. I. I. Ivanova, E. E. Knyazeva, Chem. Soc. Rev., 2013,42, 3671.
- F. N. Gu, F. Wei, J. Y. Yang, N. Lin, W. G. Lin, Y. Wang, J. H. Zhu, Chem. Mater. 2010,
   22, 2442.
- N. N. Hlaing, K.Vignesha, S. Sreekantan, S.-Y. Pung, H. Hinod, W. Kurniawan, R.Othman,
   A. A.Than, A. R. Mohamed, C. Salim, *Appli. Surf. Sci.* 2016, 363, 586.
- 13. T. Ban, T. Ohwaki, Y. Ohya, Y. Takahash, Inter. J. Inor. Mater. 1999, 1, 243.
- 14. F. Hasan, R. Singh, G. Li, D. Zhao, P.A. Webley, J. Colloid Interface Sci., 2012, 382, 1.
- 15. X.Zhang, D. Tang, G. Jiang, Adv. Powder Tech. 2013, 24, 689.
- 16. C.S.Cundy, P.A. Cox, Microporous Mesoporous Mater, 2005, 82, 1.
- 17. R. Kumar, A. Bhaumik, R. K. Ahedi, S. Ganapathy, *Nature* **1996**, 381, 298.
- A. V.Goretsky, L. W. Beck, S. I.Zones, M. E. Davis, *Microporous Mesoporous Mater.* 1999,
   387.

- P. Cubillas, M. W. Anderson, Zeolites and Catalysis, Synthesis, Reactions and Applications
   (J. Cejka, A. Corma, S. Zones), WILEY-VCH Verlag GmbH & Co, 2010, Synthesis
   mechanism: crystal growth and nucleation, 1-15.
- 20. S.L. Burkett, M.E. Davis, Chem. Mater., 1995, 7, 920.
- 21. T. Wakihara, T. Okubo, Chem. Lett., 2005, 34, 276.
- 22. J. L.Blin, C.Otjacques, G.Herrier, B.-L. Su, Langmuir, 2000, 16, 4229.
- 23. H. Kunieda, , K. Ozawa, K.L. Huang, J. Phys. Chem. B, 1998, 102(5), 831.

# PART 2

# STUDY OF CO, ADSORPTION ON IRON OXIDE DOPED MCM-41

#### 1. INTRODUCTION

It is currently accepted that carbon dioxide is one of the significant greenhouse gases that contributes to global warming.  $CO_2$  levels in the atmosphere have increased since the  $19^{th}$  century due to the vast amount of  $CO_2$  emitted through the use of carbon-based fossil fuels and other human activities. As such, the reduction of  $CO_2$  levels seems to be an important task. Several ways to reduce  $CO_2$  levels include for instance, liquid amine absorption [1-3], the use of solid adsorbents [4-6], a cryogenic technique [7, 8] and selective membrane [9, 10]. Among these techniques, liquid amine absorption is most widely used but its disadvantage is the high energy requirement for the regeneration process [11, 12]. The adsorption technology by porous materials has become of interest due to low operation costs, greater convenience and energy-efficiency in capturing  $CO_2$ .

Adsorption on solid adsorbents can undergo by one of two possible adsorption mechanisms; physical adsorption or chemical adsorption. Physical adsorption or physisorption involves intermolecular forces (van der Waals force, hydrogen bond, electrostatic force etc.) and this kind of adsorption requires a low heat of adsorption. For chemical adsorption or chemisorption, the interaction involves the valency force as a result of the sharing of electrons by the solid (adsorbent) and the substance (adsorbate). In chemisorption, the adsorbate usually binds to a certain site on the adsorbent which leads to higher heat of adsorption. CO2 adsorption mechanism is strongly dependent on the types of adsorbent materials used. Activated carbon and inorganic porous materials are normally employed to facilitate the physical adsorption process. For the chemical adsorption process, adsorbents such as metal oxides and metal salts are usually used. Metal oxides (e.g. CaO, MgO) and metal salts (e.g.Li<sub>2</sub>ZrO<sub>3</sub>, Li<sub>4</sub>SiO<sub>4</sub> etc.) have also been reported as effective chemical adsorbents [13-15]. The major physical adsorbent for CO2 adsorption are carbon, zeolite, silica and alumina. Among these materials, silica is one of the most porous adsorbents because of its high surface area, highly ordered pore structure and tunable pore sizes. Many researchers have focused on CO2 adsorption by various MCM-41 such as pore-expanded MCM-41 and modified surface of MCM-

41 [16-19]. Y. He et al.[20] investigated the heat of adsorption and adsorption heterogeneity for  $CH_4$ ,  $C_2H_4$  and  $CO_2$  on MCM-41 by calorimetric technique. They found that the adsorption of  $CH_4$  and  $C_2H_4$  on MCM-41 was homogeneous while adsorption of  $CO_2$  was heterogeneous. They proposed that the highly heterogeneous of adsorption on MCM-41 might be due to the electrostatic interactions between  $CO_2$  and the surface atoms. Another study on the effect of pressure and temperature of  $CO_2$  adsorption on MCM-41 [21] reported that  $CO_2$  adsorption capacities increased with in line with the increase  $CO_2$  pressure which was explained as  $CO_2$  being forced into MCM-41 deep pores at high pressure. On the other hand,  $CO_2$  adsorption decreased with a lowering of adsorption temperature. The decrease of adsorption was suggested to be due to the weakening of the van der Waals forces between MCM-41 and  $CO_2$ . In conclusion, the interaction between  $CO_2$  and the MCM-41 adsorbent was physical adsorption.

CO<sub>2</sub> molecules have a soft acidic nature; therefore the presence of basicity sites on the surface of metal oxide can enhance CO<sub>2</sub> adsorption capacity. The use of metal oxide modified on mesoporous materials has been one of the promising ways to increase CO<sub>2</sub> adsorptive properties. However, the metal carbonate formation of these metals after adsorption process requires significantly high energy to decompose to metal oxide in the regeneration step [22]. The improvement of the adsorptive properties of mesoporous materials by transition metal species such as copper oxide, nickel oxide, chromium oxide, iron oxide, bismuth oxide, lanthanum oxide and cerium oxide have been reported to be effective for CO<sub>2</sub> adsorption and require low regeneration energies [23-28]. However, there are few studies on the adsorption behavior or adsorption mechanism of CO<sub>2</sub> on these transition metal oxides. It is therefore of interest in this study

In this work, iron oxide was introduced to mesoporous MCM-41hich was characterized by  $N_2$  adsorption-desorption, scanning electron microscopy and  $CO_2$  adsorption isotherm. The  $CO_2$  adsorption and the adsorption mechanism were studied by in-situ  $CO_2$  adsorption technique. X-ray absorption near edge was used to determine the oxidation state of iron oxide during the  $CO_2$  adsorption process and to investigate the movement of electron densities between adsorbate and adsorbent by comparing the white line intensities of XANES spectra.

# 2. EXPERIMENT

#### 2.1 Sample preparation

# 2.1.1 Preparation of MCM-41

Mesoporous MCM-41 was synthesized by gelation which was also used by Melendez-Ortiz et. al. [29]. In the preparation procedure, 0.5 g of cetyltrimethylammonium bromide (CTAB) was dissolved in 96 mL of DI water. After obtaining a clear solution, 34 mL of ethanol was added dropwise to the mixture while stirring. After stirring for 5 min., 2 mL of tetraethyl orthosilicate (TEOS) was poured into the solution. The solution was continuously stirred for 3 hours at room temperature. The synthesized powder was filtered, washed with DI water and dried overnight at room temperature. Finally, the powder was calcined at 540 °C for 9 hours to remove the organic template.

# 2.1.2 Preparation of iron oxide/MCM-41 adsorbents

For the iron impregnation procedure, the synthesized mesoporous silica was immersed in a solution of  $Fe(NO_3)_3 \cdot 9H_2O$ . Urea solution was added in order to disperse the doped metal onto the silica surface [30] and then the mixture was stirred for 12 hours at room temperature. The slurry was dried at 100  $^{\circ}C$  with vigorous stirring. The obtained powder was calcined at 460  $^{\circ}C$  for 6 hours. The final powder was denoted as x%Fe/MCM-41 (x = 0.10, 0.25, 0.50, 0.75 and 1.0 wt%)

#### 2.2 Characterization

XRD patterns of MCM-41 and doped samples were obtained from Bruker D8 advance diffractometer with Cu K $_{\alpha}$  radiation. The diffraction spectra were recorded in the range of 2 $\theta$  = 1 $^{\circ}$  - 40 $^{\circ}$ .

 $N_2$  adsorption-desorption isotherms were obtained on an Autosorb 1-C instrument (Quantachrome) at-196 °C. Prior to measurement, the samples were degassed under vacuum at 300 °C for 3 hours. The specific surface areas of all samples were determined by the multipoint BET method and average pore volume and diameter were obtained at relative pressure  $(P/P_o) \approx 1$ . Pore size distributions were calculated by the BJH method from the adsorption branch of the isotherms.

The synthesized adsorbents morphology was observed by scanning electron microscope (LEO model 1450VP) with an accelerating voltage of 20 kV.

# 2.3 CO<sub>2</sub> adsorption

 ${
m CO_2}$  adsorptions of all synthesized adsorbents were performed on a NOVA 1200 e instrument (Quantachrome) at the desired temperature. About 200 mg of samples were outgassed at 300  $^{\circ}{
m C}$  for 3 hours in vacuum prior to adsorption measurement.

# 2.4 X-ray absorption spectroscopy

X-ray absorption spectroscopy measurements were carried out in X-ray absorption near edge structure (XANES) region on Time-resolved X-ray absorption spectroscopy (TRXAS) end-station at the Synchrotron Light Research Institute (SLRI), Nakhonrachasima, Thailand [31]. The electron storage ring was operated at 1.2 GeV. The bent crystal was used as an energy dispersive monochromator. The Si(111) crystal was used as a bent crystal with an energy range of 2.4 - 10 keV. The detector was a linear image sensor. The XANES spectra were recorded in K absorption edge of Fe. The oxidation state of Fe on MCM-41 was determined first. The Fe compound with various oxidation state; Fe foil, FeO, Fe<sub>2</sub>O<sub>3</sub> and Fe<sub>3</sub>O<sub>4</sub>, were used as a standards. This experiment was done in order to explore the oxidation state of Fe before using for in-situ CO2 adsorption process. The sample was deposited over the Kapton tape which was placed on the sample frame. The incident beam (Io) was detected without the sample and the transmitted beam (I<sub>1</sub>) was detected by transmitting light from the sample. The XANES spectra were obtained by subtracting of I<sub>1</sub> by I<sub>o</sub> with the preprocessing programed which produced by Beamline 2.2 before being imported to the data analysis program. Data analysis was carried out by pre-edge background removal and normalized by division of the height of the absorption edge. The software Athena was used to process the data reduction.

For time-resolved in-situ  $CO_2$  adsorption experiment, the sample was pressed into a pellet and placed in an in-situ cell and heated with a heating rate of 2  $^{\circ}$ C/min from room temperature to 300  $^{\circ}$ C. Fe K-edge XANES spectra during  $CO_2$  adsorption (flow rate = 5 mL/min) were recorded at room temperature and the spectra were collected every minute for 20 minutes.

#### 3. RESULTS AND DISCUSSION

#### 3.1 Materials characterization

Powder X-ray diffraction measurements were used to obtain the information about changes of the MCM-41 structure upon impregnation of iron oxide. Small angle XRD patterns of MCM-41, 0.5wt%Fe/MCM-41 and 1.0wt%Fe/MCM-41 are displayed in Figure 1. All of the samples exhibited three characteristic diffraction peaks, which corresponded to the planes (100), (110), (200) of the hexagonal regularity of MCM-41 [29]. The diffraction peaks of iron oxide phase was not observed in all doped samples as shown in wide angle XRD spectra (inset). These results indicates that the hexagonal array of mesopore in MCM-41 was sustained after the introduction of iron and suggests that the doped oxide species was highly dispersed on the MCM-41 surface [32].

Figure 2 shows the nitrogen adsorption-desorption isotherm of MCM-41 and 0.5wt% Fe doped MCM-41. For the isotherm of MCM-41, it was found that the isotherm is a typical type IV [29]. A steep increase in the nitrogen uptake from 0.20-0.35 indicates the occurrence of mesoporous with a narrow pore size distribution. In the case of doped sample (0.50wt%), the type IV of adsorption isotherm was also found. The pore size distribution calculated for both samples using the BJH method are shown in Figure 3. These two samples exhibit a pore size in a mesoporous range (2.25-2.50 nm). The pore size of the doped sample was not different from the undoped sample. The BET surface area, pore diameter and pore volume of all adsorbents are summarized in Table 1. The BET surface area of MCM-41 is in agreement with previous work reported for mesoporous MCM-41 [29]. The information from the table showed that the surface area of the doped sample decreased with the increase of metal content except 0.50wt%. The addition of metal on to the MCM-41 surface by an impregnation method led to some pore blocking and then a lowering of the surface area and then pore volume and pore diameter were enlarged.

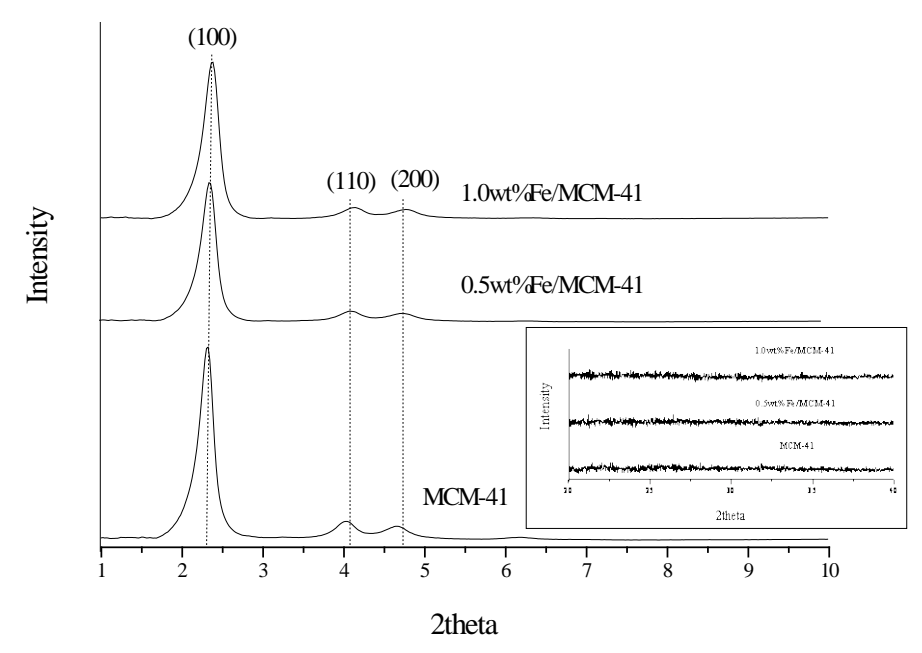


**Fig. 1.** XRD patterns of MCM-41, 0.5 wt%Fe/MCM-41 and 1.0 wt%Fe/MCM-41. The inset shows wide angle XRD patterns of corresponding samples.

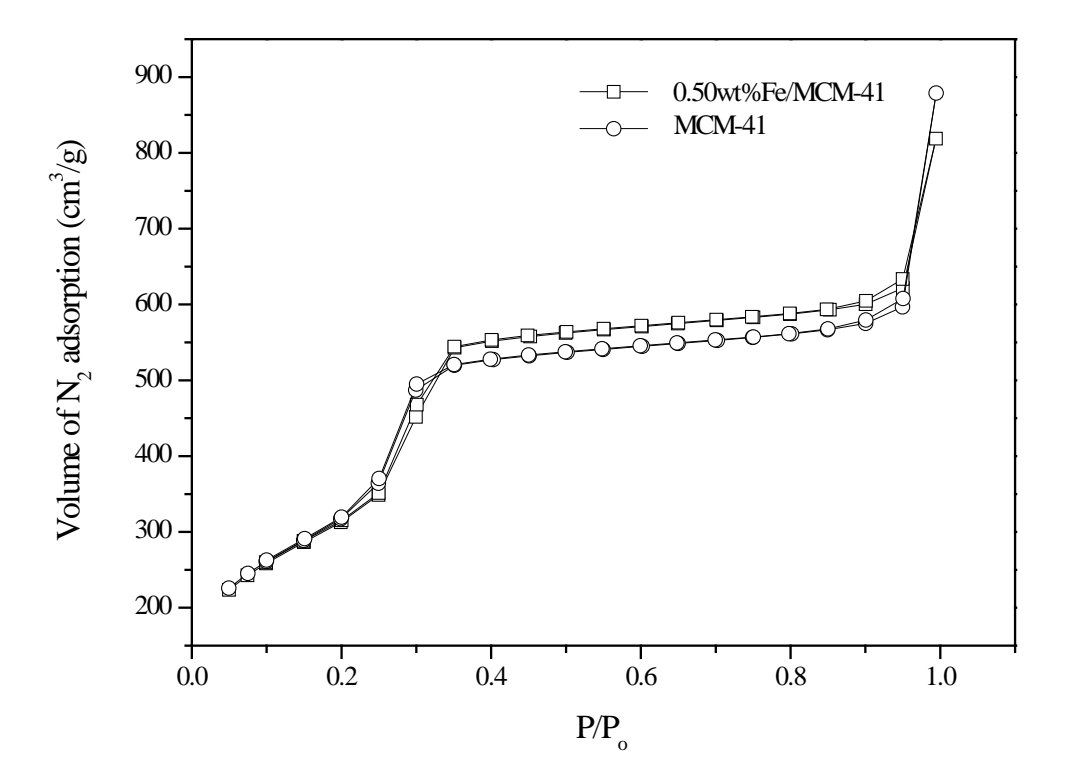


Fig. 2.  $\ensuremath{N_2}$  adsorption-desorption isotherms of MCM-41 and 0.50 wt%Fe/MCM-41.

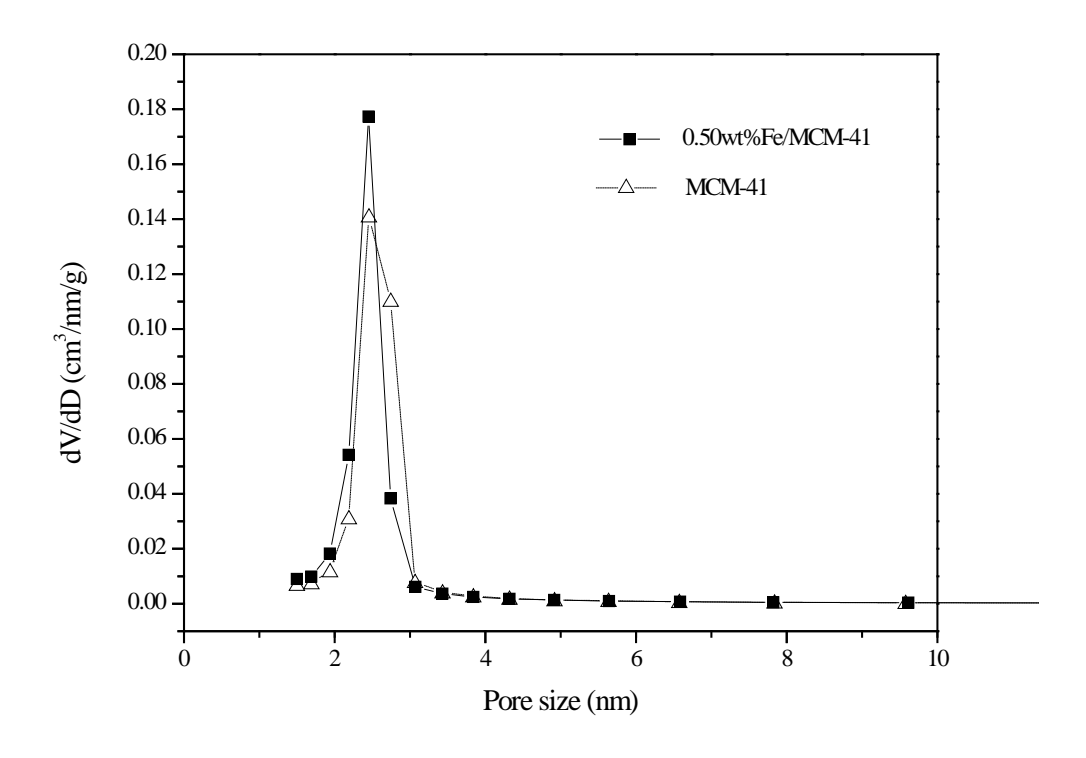


Fig. 3. Pore size distributions of MCM-41 and 0.50 wt%Fe/MCM-41.

Table 1 Summarization of surface area, pore diameter and pore volume of all samples.

Camples	S <sub>BET</sub>	Average pore diameter	Pore volume
Samples	(m <sup>2</sup> /g)	(nm)	(cm <sup>3</sup> /g)
MCM-41	1530	3.32	1.27
0.10wt%Fe/MCM-41	1491	3.19	1.19
0.25wt%Fe/MCM-41	1506	3.36	1.26
0.50wt%Fe/MCM-41	1548	3.52	1.36
0.75wt%Fe/MCM-41	1515	3.40	1.29
1.0wt%Fe/MCM-41	1453	3.12	1.11

The SEM micrograph of the mesoporous MCM-41 and doped MCM-41 are shown in Figure 4. From figure 4(a), it can be observed that the MCM-41 has a spherical morphology. These spherical particles are uniform and the particle size is between 200-300 nm. In the case

of 0.50wt%Fe/MCM-41, the morphology of the particle is slightly distorted from a spherical shape (i.e. rod like structure) with a similar particle size to that of MCM-41.

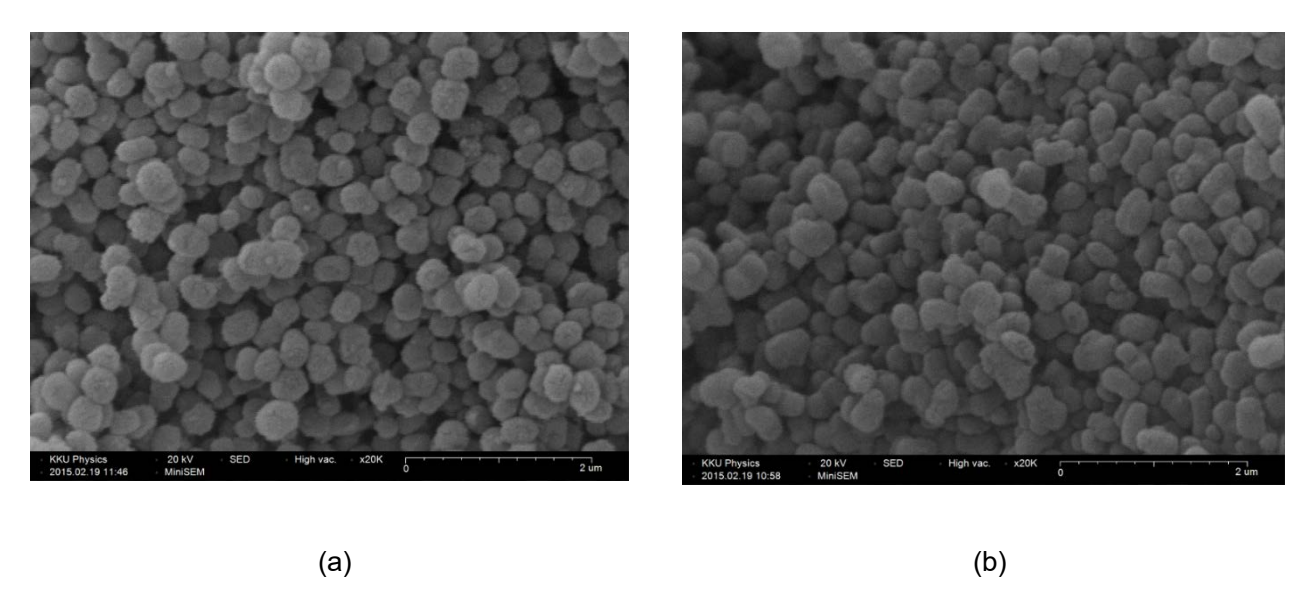
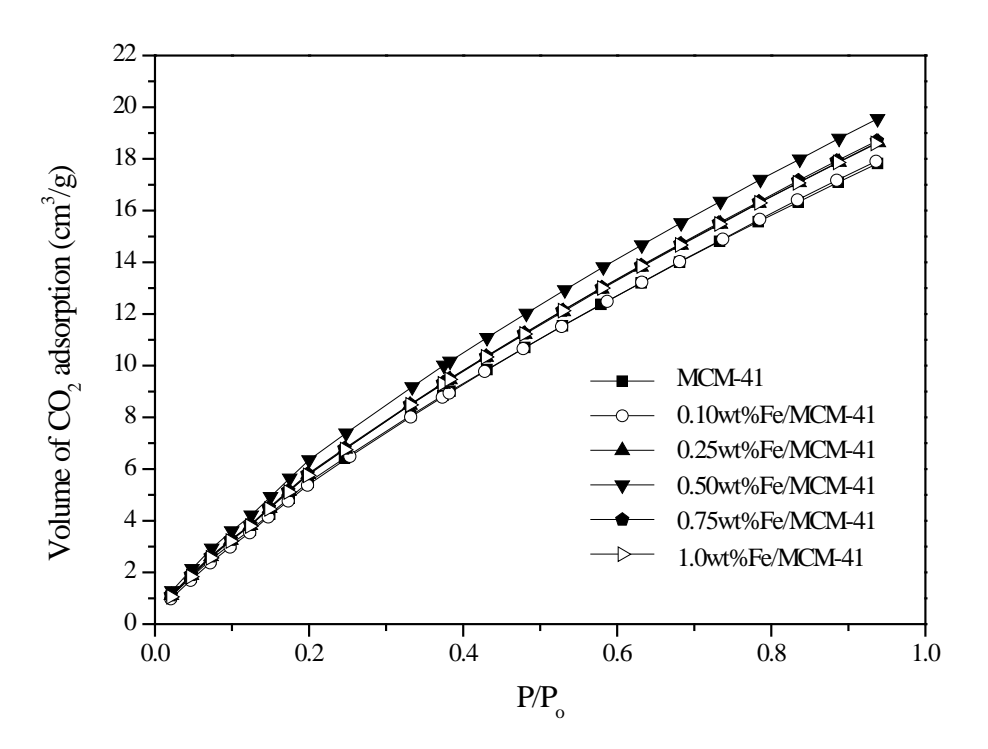


Fig. 4. Scanning electron micrograph of (a) MCM-41 and (b) 0.50 wt%Fe/MCM-41.

# 3.2 CO<sub>2</sub> adsorption isotherm

The  ${\rm CO}_2$  adsorption isotherms of MCM-41 and 0.50wt%Fe/MCM-41 at 25  $^{\circ}$ C are shown in Figure 5. The  ${\rm CO}_2$  adsorption capacity increases with the increase of  ${\rm CO}_2$  pressure. Maximum adsorption (P/P $_{\rm o}$  $\approx$ 1) was found to be 19.55 cm $^3$ /g for 0.50wt%Fe/MCM-41 while that of MCM-41 was 17.82 cm $^3$ /g.

Figure 6 illustrates the correlation between the volume of CO<sub>2</sub> adsorbed and BET surface area. Maximum adsorption is found with 0.5wt%Fe/MCM-41. It can be clearly seen that the extent of adsorption is related to the BET surface area. Therefore, 0.50wt%Fe/MCM-41was selected to further study the CO<sub>2</sub> adsorptive behavior.



**Fig. 5.** Adsorption isotherms of MCM-41 and x%Fe/MCM-41 (x  $\upmu$  0.10, 0.25, 0.50, 0.75 and 1.0 wt%) at 25  $^{\circ}$ C.

The isosteric heat of adsorption (Q<sub>st</sub>) can be used to describe the strength of adsorbate-adsorbent interaction [33]. The isosteric heat of adsorption for CO<sub>2</sub> adsorption on doped adsorbents was obtained by the Clausius-Clapeyron equation as

$$\left(\frac{\partial(\ln P_{CO_2})}{\partial(1/T)}\right) = \frac{Q_{st}}{R} \tag{1}$$

Where  $P_{CO_2}$  is the  $CO_2$  partial pressure, T is the absolute temperature and R is the gas constant. If the  $Q_{st}$ , for a given amount of adsorbed gas, is temperature-independent, then the plots of InP against 1/T should yield a straight line. Generally, heats of adsorption are in the range of 60-90 kJ/mol for chemisorption and 25-50 kJ/mol for physisorption [34]

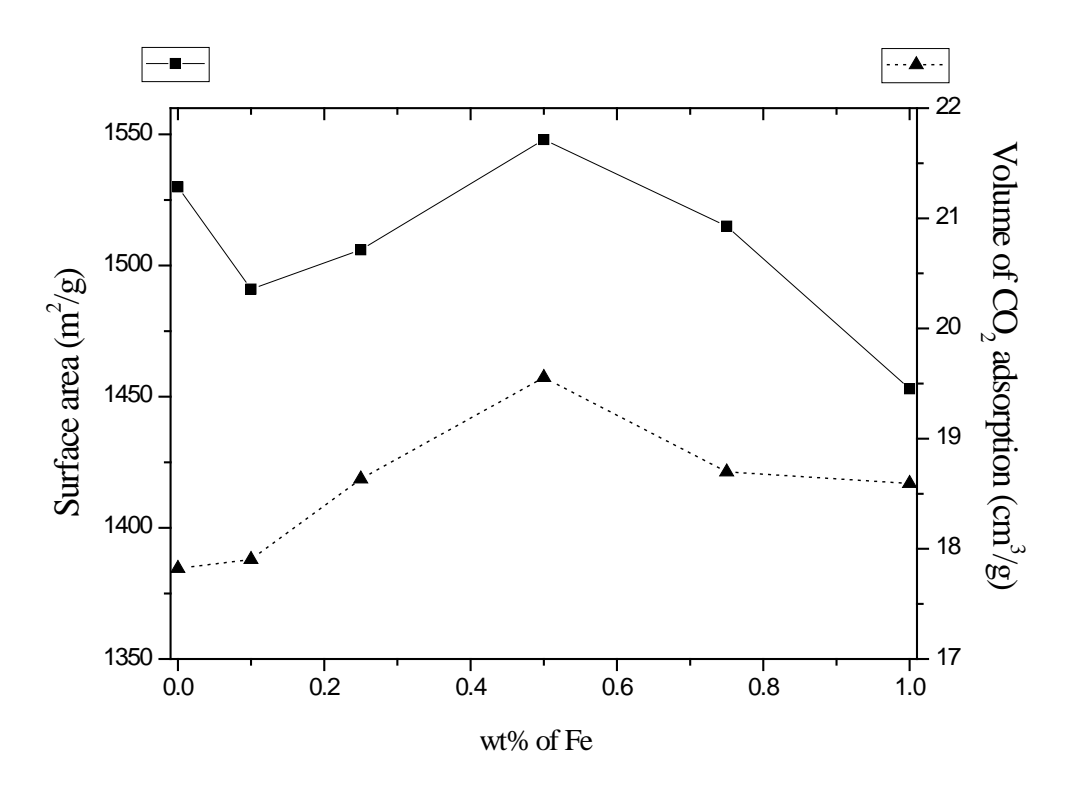
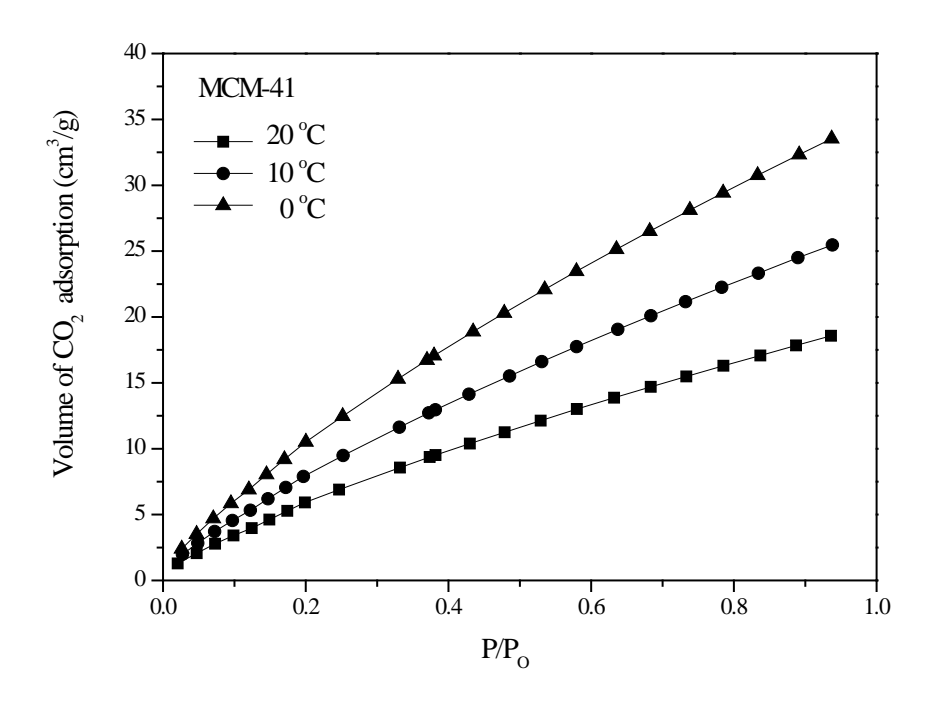


Fig. 6. Correlation between volumes of  ${\rm CO_2}$  adsorbed at P/Po z 1 and surface area.

Figure 7(a) and (b) illustrates the  ${\rm CO_2}$  adsorption isotherms of MCM-41 and 0.50wt%Fe/MCM-41 at multiple temperatures, respectively. It is obvious that the  ${\rm CO_2}$  adsorption capacity decrease with the increase of adsorption temperature. The deduction of the adsorption isotherm at various adsorbed volume led to the plot between  ${\rm ln\,P_{\rm CO_2}}$  vs 1/T and the slope of this straight line was the isosteric heat of adsorption. The isosteric heat of adsorption of 0.50wt%Fe/MCM-41 is -25.97 kJ/mol while that of MCM-41 was -21.53 kJ/mol. The more negative isosteric heat of adsorption indicated that there was a stronger binding between adsorbate and adsorbent. These  ${\rm Q_{st}}$  indicate that the adsorption process is exothermic which is in agreement with the results of adsorption isotherm and the interaction between  ${\rm CO_2}$  and adsorbent was physical adsorption.



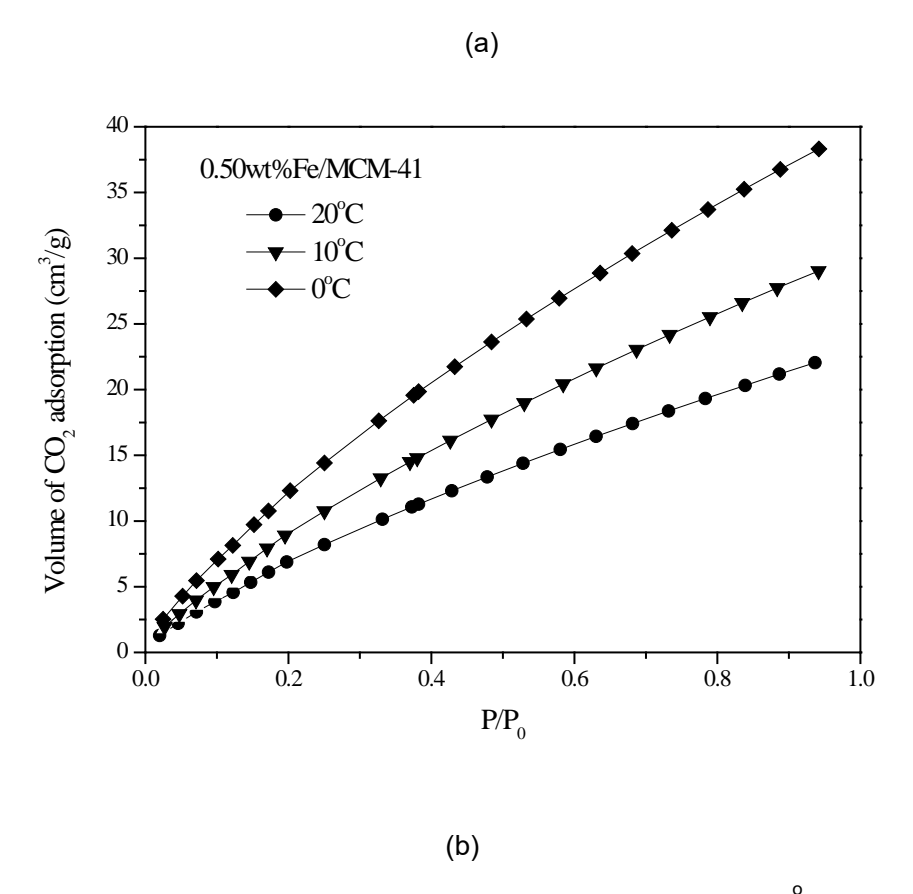


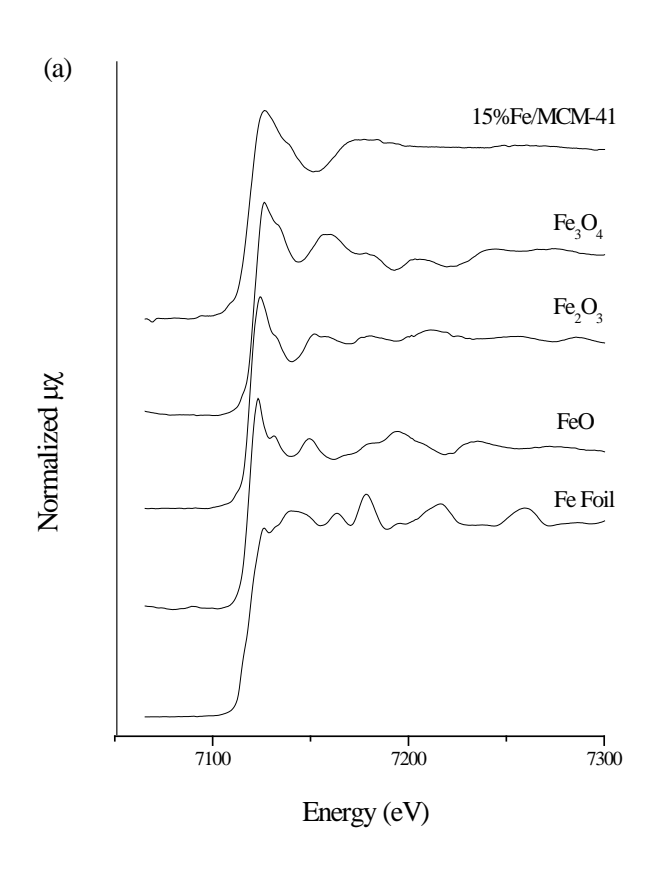
Fig. 7. (a)  $CO_2$  adsorption on MCM-41 at 0, 10 and 20  $^{\circ}$ C. (b)  $CO_2$  adsorption on 0.5 wt%Fe/MCM-41 at 0, 10 and 20  $^{\circ}$ C.

# 3.3 X-ray absorption spectroscopy

The most widely used method for investigating the adsorbed species on surface in the adsorption process is infrared spectroscopy, especially in-situ infrared spectroscopy. However X-ray absorption spectroscopy (XAS) is an interesting technique used to monitor the interaction between adsorbate and adsorbent to see whether there are some electron movements between them. This technique can also be used to study the role of doped metal oxide in enhancing the CO<sub>2</sub> adsorption capacity. The XANES technique was used in this study to monitor the oxidation state and d-electron density of iron oxide on MCM-41 during the CO<sub>2</sub> adsorption process. It is worth mentioning that for the XANES technique, a high concentration of doped metal is needed in order to obtain an appropriate spectra and this technique is not sensitive for low metal content.

#### 3.3.1 Oxidation state of Fe

Figure 8(a) shows XANES spectra recorded at the Fe K absorption edge for standard Fe metal, FeO, Fe<sub>2</sub>O<sub>3</sub>, Fe<sub>3</sub>O<sub>4</sub> and 5%Fe/MCM-41. XANES spectra for standard Fe<sub>2</sub>O<sub>3</sub> exhibit an absorption of K edge at 7131 eV which characterized the iron in trivalent state while that of FeO in divalent state was observed at 7134 eV. The K absorption edge is caused by the ejection of Fe 1s electrons after absorption of a photon [35]. The oxidation state of iron doped samples can be obtained by differentiating the XANES spectra and assigning the turning point of the derivative spectra as the edge energy. Figure 8(b) illustrates the plot of edge energy shift of Fe<sup>2+</sup>, Fe<sup>3+</sup> (K absorption edge) relative to edge energy of Fe<sup>o</sup>. The edge energy shift of 5%Fe/MCM-41 when placed on the straight line indicated that the oxidation state of Fe in the doped sample was 3. These results indicate that the doped iron is in oxide form and its apparent oxidation state is 3. The form of doped iron species should be oxide form due to a calcination procedure was carried out under atmospheric pressure. It is seen that the extended part of the XANES spectra of doped sample exhibits an oscillation different from other iron oxide reference compounds (FeO, Fe<sub>2</sub>O<sub>3</sub> and Fe<sub>3</sub>O<sub>4</sub>). To determine the actual configuration and environment of doped iron oxide, proper modeling of XANES spectra is needed; hence, it is of interest to study further. From XANES spectra, it can be preliminary concluded that the doped iron species oxidation state is +3 and should be in oxide (FeOx) form due to a calcination process.



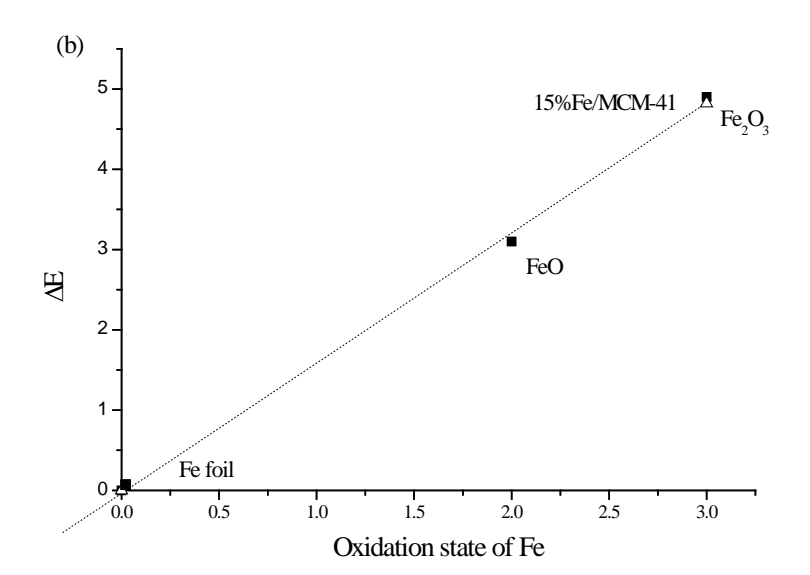


Fig. 8. (a) XANES spectra of the Fe K absorption edge for Fe foil, FeO, Fe<sub>2</sub>O<sub>3</sub>, Fe<sub>3</sub>O<sub>4</sub> standards and 5 wt%Fe/MCM-41.

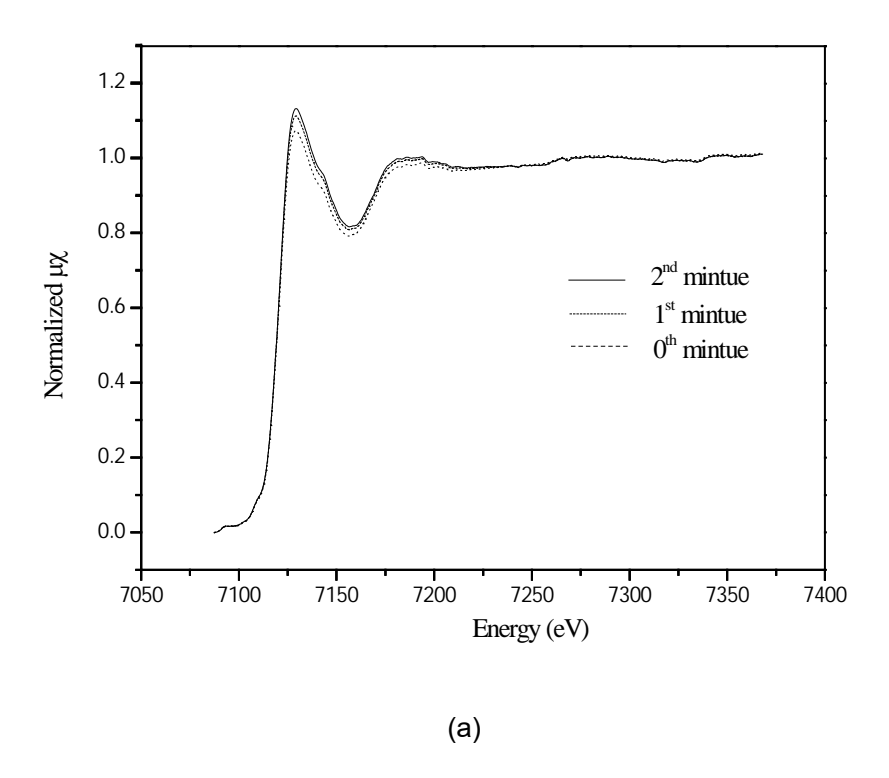
(b) Relationship between edge energy shift of Fe standard and the oxidation states.
Filled squares are Fe foil, FeO and Fe<sub>2</sub>O<sub>3</sub> standards, open triangles is 5
wt%Fe/MCM-41.

### 3.3.2 Time-resolved CO2 adsorption

Figures 9(a) and (b) display time-resolved XANES spectra during the CO<sub>2</sub> adsorption process for 20 mins for 5wt%Fe/MCM-41. The white line intensity was compared to investigate the interaction between the adsorbed gas and the doped metal oxide. In our previous works [36, 37], we used the comparison of the white line intensities of XANES spectra to describe the role of doped metal in enhancing WGS activity. The intensity of the white line is related to the occupancy of the d-state of the element. A highly occupied d-state means that fewer core electrons can be excited into its d-state. Therefore, the intensity of the absorption peak is low. In contrast, if the d-state is only slightly occupied, more core electrons can be excited and move into it, and so the absorption peak is strong.

Figure 9(a) shows the comparison of white line intensities of Fe K absorption edge at zeroth minute and the first two minutes. In this figure, the white line intensity of 5wt%Fe/MCM-41 at the first minute is slightly higher than that of the doped absorbent at the zeroth minutes and that of the second minute is also slightly higher than that of the first minute. After the third minute, the sizes of the white line stay the same as that of the second minute (Figure 9(b)).

These spectra indicated that  $CO_2$  can be rapidly adsorbed (within 2 minutes) on an iron oxide doped MCM-41 surface and that during the adsorption process, some electrons moved out of iron d-orbitals. The oxidation states of Fe during the  $CO_2$  adsorption process were determined by a plot similar to Figure 8 and the results indicated that the oxidation state of Fe during the adsorption process was slightly higher than +3. The loss of electrons from the d-state of the Fe indicates the transfer of d-electrons into the  $\pi^*$ -antibonding orbital of  $CO_2$  during the adsorption process.



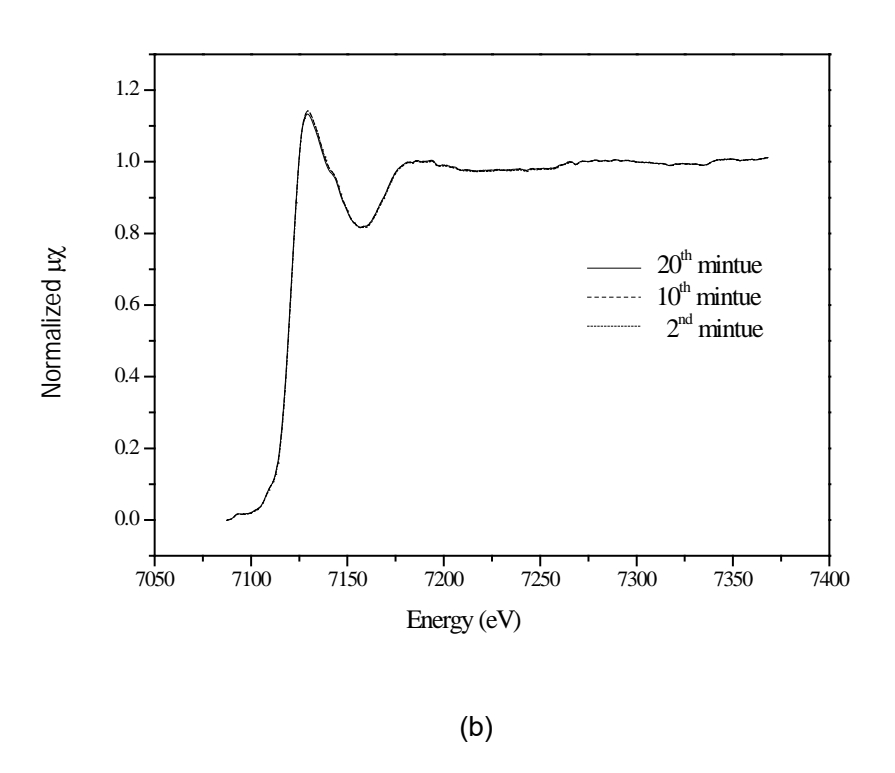


**Fig. 9.** White line intensities comparison for 5 wt%Fe/MCM-41. (a) 0th, 1<sup>st</sup> and 2<sup>nd</sup> minutes (b) 2nd, 10th and 20th minutes.

#### 3.4 The adsorbed state of CO,

Few papers have reported on the adsorbed state of CO<sub>2</sub> onto the adsorbent surface and those works have mostly been done by using infrared spectroscopy. CO<sub>2</sub> is an amphoteric molecule and it is usually used as a probe molecule to test the basicity of metal oxides. The configuration of CO<sub>2</sub> upon adsorbing onto the metal oxide surface can be either linear or bent. J.A. Rodriguez [38] suggested that CO<sub>2</sub> is a net donor of electrons when adsorbed in a linear form and a net acceptor upon adsorption in a bent form.

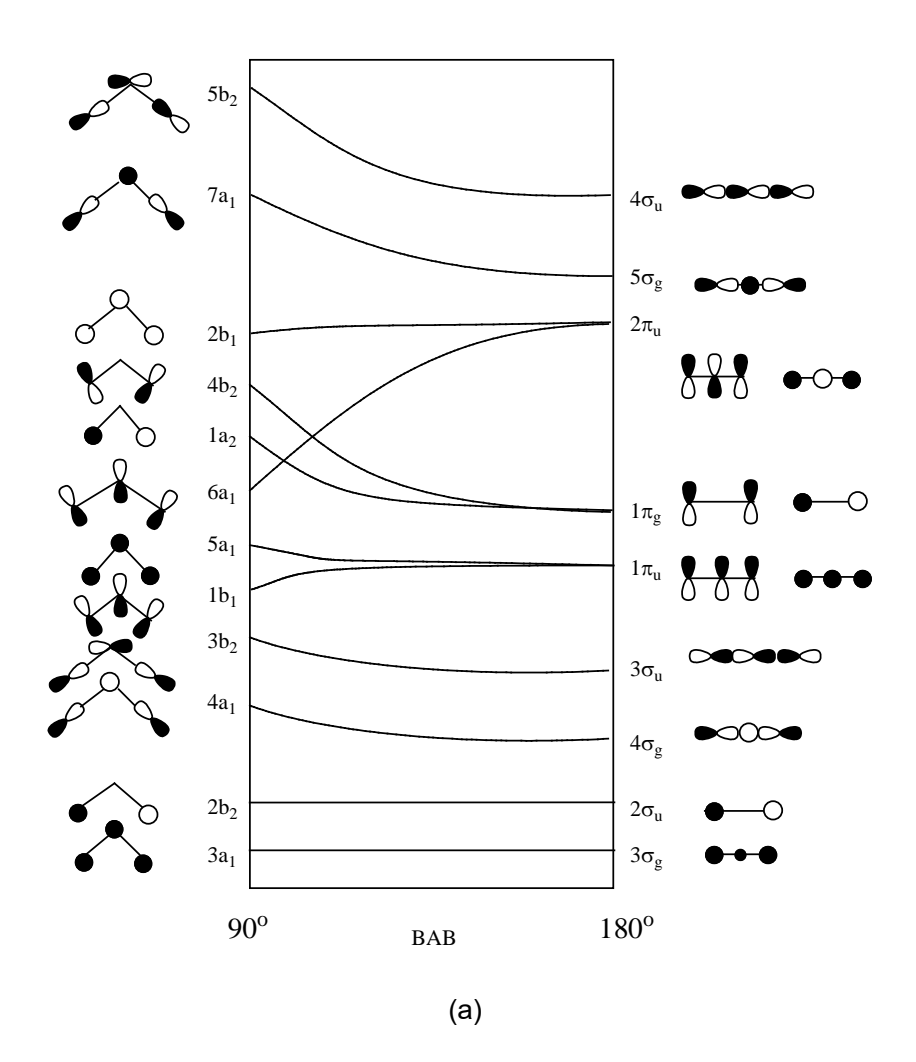
The electronic structure of  $CO_2$  can be represented by a molecular orbital diagram as shown in Figure 10(a). The formation of  $CO_2$  molecules are as follows: 2s and 2p atomic orbital of carbon and oxygen are contributed to form molecular orbitals. In linear  $CO_2$  formation, three 1s atomic orbitals of carbon and oxygen are unchanged when forming the molecule and become molecular orbitals as  $1\sigma_g$ ,  $2\sigma_g$  and  $1\sigma_u$ . The 2s atomic orbitals of carbon and  $2p_z$  atomic orbital of oxygen are directly mixed along the molecular axis and give three molecular orbitals of  $\sigma$  symmetry which are labelled as  $3\sigma_g$ ,  $4\sigma_g$  and  $5\sigma_g$ . In the same way,  $2p_z$  atomic orbitals of carbon and oxygen can form three molecular orbitals with  $\sigma$  symmetry as  $2\sigma_u$ ,  $3\sigma_u$  and  $4\sigma_u$ . The  $2p_x$  and  $2p_y$  atomic orbitals of carbon and oxygen can form six molecular orbitals with three doubly degenerated  $\pi$ -orbitals labelled as  $1\pi_g$ ,  $1\pi_u$  and  $2\pi_u$ .

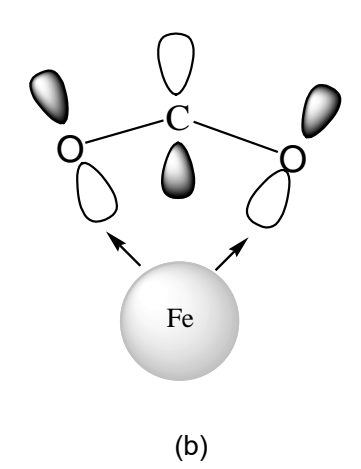
There are 22 electrons which could be filled into molecular orbitals. First, the six electrons occupy the core 1s orbitals. The remaining 16 valence electrons are distributed into four  $\sigma$  orbitals (eight electrons) and two degenerated  $\pi$ -orbitals (eight electrons). The six occupied molecular orbitals can be divided as two  $\sigma$  of C-O bond ( $3\sigma_g$ ,  $2\sigma_u$ ) and two  $\sigma$  lone pairs ( $4\sigma_g$ ,  $3\sigma_u$ ). The  $1\pi_u$  represented the  $\pi$  of C-O bond and  $1\pi_g$  are  $\pi$  lone pairs. Figure 10(a) illustrates the energy level of linear geometry and that of bent geometry upon the changing of the  $CO_2$  structure. It appears that all of the  $\sigma$ -orbital energies slightly increase or are unchanged from linear to bent configuration. In contrast, the  $\pi$ -orbital energies show obvious alterations; in particular the degeneracies of  $\pi$ -orbitals for bent molecules are split. Figure 10(a) shows a little splitting of  $1\pi_u$  and  $1\pi_g$ ; however, for  $1\pi_g$  the orbital energy increase upon changing to a bent structure and this can be attributed to the fact that linear

geometry is more favorable. For the  $2\pi_u$ , the splitting becomes  $2b_1$  and  $6a_1$ . The energy of  $2b_1$  is almost the same while that of  $6a_1$  falls sharply in the bent molecule. The occupation of  $2\pi_u$  and  $6a_1$  molecular orbitals are important to determine the bonding angles of  $CO_2$  since this is only the valance orbital which the bent molecule strongly favored [39]. Evidence from the time-resolved in-situ  $CO_2$  adsorption experiment indicated the transfer of metal d-electrons into the  $2\pi_u$  of  $CO_2$ . In order to lower the energy the  $CO_2$  configuration must change from linear to slightly bent as described in Figure 10(b). The results from the isosteric heat of adsorption of  $CO_2$  on MCM-41 and Fe/MCM-41 indicated that the interaction between  $CO_2$  and solid adsorbent were physical adsorption since their interaction were explained by van der Waals force.

The increase of CO<sub>2</sub> adsorption on modified MCM-41 can be explained by two factors, i.e., increases of BET surface area and electron transfer from metal d-orbital. X-ray crystallography indicated that iron atoms were highly dispersed on the MCM-41 surfaces. Particle analysis indicated the increases of pore volume and surface area. Good correlations between the amount of CO2 adsorption and the surface area were observed. Therefore, the increases of CO<sub>2</sub> adsorption can partly be attributed to the increase of the surface area. However, the increase of isosteric heat of adsorption indicated strong bonding between CO2 and the adsorbate. This observation can be explained by X-ray absorption spectroscopy. From the oxidation state determination, the iron atom exhibited the oxidation state of slightly higher than +3 which indicated movement of small amounts of electrons away from  ${\rm Fe}^{^{3+}}$  center. Timeresolved XANES spectra of Fe during CO2 adsorption on the modified MCM-41 showed that the adsorption process completed within 2 minutes and the slight enlargement of the white line indicated a movement of electrons out of the metal d-orbitals. We presumed that it is the movement of the metal d-electron into the empty  $CO_2$  antibonding  $2\pi_u$  leading to slightly bent CO2 adsorbate. This electron transferring process gave rise to stronger metal-adsorbate bonding as indicated by the increase of the isosteric heat of adsorption. From all of these evidences, we concluded that the enhancement of CO2 adsorption on iron oxide modified MCM-41 was partly due to the increase of surface area and partly by the electron transfer

between iron d-orbital and  ${\rm CO_2}$  antibonding  $2\pi_{\rm u}$ . However, the configuration of  ${\rm CO_2}$  upon adsorption needs to be further studied by using other techniques.





- **Fig. 10.** (a) Walsh diagram of CO<sub>2</sub> orbital energies for linear and bent geometries.
  - (b) Proposed adsorption mechanism of CO<sub>2</sub> and dope iron oxide.

#### 4. CONCLUSION

 ${
m CO_2}$  adsorption of iron oxide doped on mesoporous MCM-41 was studied and the results showed that the  ${
m CO_2}$  adsorption capacity of 0.50wt%Fe/MCM-41 was higher than that of the undoped MCM-41. The characteristic results from XRD,  ${
m N_2}$  adsorption-desorption and SEM revealed that the mesoporous structure and morphology of iron oxide doped MCM-41 were not different from the starting mesoporous material. The isosteric heat of adsorption indicated that the interaction between  ${
m CO_2}$  and iron oxide doped MCM-41 was physical adsorption. The enhanced  ${
m CO_2}$  adsorption of iron oxide doped MCM-41 was attributed partly to the increase of surface area and partly to electron transfer from metal d-orbital to  ${
m CO_2}$  antibonding  $2\pi_u$ . This experiment gave an insight to the techniques that may be used to improve  ${
m CO_2}$  adsorption upon the modified adsorbate.

#### **Acknowledgements**

We would like to thank the Center of Excellence for Innovation in Chemistry (PERCH-CIC), Materials Chemistry Research Center, Khon Kaen University, Thailand Research Fund: Grant No. MRG5980081, and Commission on Higher Education, Ministry of Education for financial support. Generous beam time from the Synchrotron Light Research Institute (SLRI) is gratefully acknowledged.

#### References

- [1] K. K. P. Akanksha, V. K. Srivastava, Chem. Eng. J., 133 (2007) 229-237.
- [2] A. Samanta, S. S. Bandyopadhyay, Chem. Eng. Sci., 64 (2009) 1185-1194.
- [3] F. Shakerian, K.-H. Kim, J. E. Szulejko, J.-W. Park, Appl. Energy, 64 (2015) 10-22.
- [4] A. Anson, C. C. H. Lina, S. M. Kuznickia, J. A. Sawadab. *Chem. Eng. Sci.*, 64 (2009) 3683-3687.
  - [5] H. An, B. Feng, S. Su, Int. J. Greenh. Gas Con., 5 (2011) 16-25.
  - [6] G. Zhao, B. Aziz, N. Hedin, Appl. Energy, 87 (2010) 2907-2913.

- [7] K. E. Zanganeh, A. Shafeen, C. Salvador, Energy Procedia, 1 (2009) 247-252.
- [8] C.-F. Song, Y. Kitamura, S.-H. Li, W.-Z. Jiang, *In.t J. Greenh. Gas Con.*, 13 (2013) 26-33.
  - [9] A. Brunetti, F. Scura, G. Barbieri, E. Drioli. J. Membr. Sci., 359 (2010,) 115-125.
- [10] P. Luis, T. V. Gerven, B. V. Bruggen, Prog. Energy Combust. Sci., 38 (2012) 419-448.
- [11] X. Xu, C. Song, J. M. Andrésen, B. G. Miller, A. W. Scaroni, *Microporous Mesoporous Mater.*, 62 (2003) 29-45.
- [12] F. Zheng, D. N. Tran, B. J. Busche, G. E. Fryxell, R. S. Addleman, T. S. Zemanian, C. L. Aardahl, *Ind. Eng. Chem. Res.*, 44 (2005) 3099-3015.
- [13] H. Jeona, Y. J. Min, S. H. Ahna, S.-M. Hong, J.-S. Shin, J. H. Kima, K. B. Lee, Colloids Surf. A: Physicochem. Eng. Asp., 414 (2012) 75-81.
  - [14] H. R. Radfarnia, A. Sayari, Chem. Eng. J., 262 (2015) 913-920.
- [15] A. Akgsornpeak, T. Witoon, T. Mungcharoen, T. Limtrakul, *Chem. Eng. J.*, 23 (2014) 189-198.
  - [16] S. Loganathan, A. K. Ghoshal, Chem. Eng. J. 308 (2017) 827–839.
  - [17] S. Ahmed, A. Ramli, S. Yusup, Int. J. Greenhouse Gas Control 51 (2016) 230–238.
- [18] N. E. Taria , A. Tadjarodia , J. Tamnanloob , S. Fatemi, *J. CO*<sub>2</sub> *Util.* 14 (2016) 126–134.
  - [19] Z. Liu, Y. Teng, K. Zhang, H. Chen, Y. Yang, J. Energy Chem. 24(2015)322–330.
  - [20] Y. He, N. A. Seaton, Langmuir 22 (2006) 1150-1155.
  - [21] A. Ramli, S. Ahmed, Y. Suzana, Chem. Eng. Trans. 39 (2014) 271-276.
- [22] W. N. R. W. Isahak, Z. A. C. Ramli, M. W. Ismail, K. Ismail, R. M. Yusop, M. W.
   M. Hisham, M. A. Yarmo, J. CO<sub>2</sub> Util. 2 (2013) 8–15.
  - [23] D. I. Jang, S. J. Park, Fuel, 102 (2012) 439-444.
  - [24] M. W. Abee, S. C. York, D. F. Cox, J. Phys. Chem. B, 105 (2001) 7755-7761.
- [25] J. Baltrusaitis, J. Schuttlefield, E. Zeitler, V. H. Grassian, *Chem. Eng. J.*, 170 (2011) 471-481.
  - [26] T. Esaka, K. Motoike, J. Alloys Compd., 408-412 (2006) 480-483.
  - [27] S. C. Shen,, X. Chen, S. Kawi, Langmuir, 20 (2004) 9130-9137.

- [28] K. Yoshikawa, H. Sato, M. Kaneeda, J. N. Kondo, J. CO, Util., 8 (2014) 34-38.
- [29] H. I. Mele'ndez-Ortizn, L. A. Garcı'a-Cerda, Y. Olivares-Maldonado, G. Castruita, J. A. Mercado-Silva, Y. A. Perera-Mercado, *Ceram. Inter.*, 38 (2012) 6353-6358.
  - [30] H. Zhao, W. Yan, Z. Bian, J. Hu, H. Liu. Solid State Sci., 14 (2012) 250
  - [31] Y. Poo-arporn, P. Chirawatkul, W. Saengsui, S. Chotiwan, S. Kityakarn, S.
- Klinkhieo, J. Hormes, P. Songsiriritthigul, J. Synchrotron Radiat., 19 (2012) 937-943.
- [32] R. Kohn, D. Paneva, M. Dimitrov, T. Tsoncheva, I. Mitov, C. Minchev, M. Froba. *Microporous Mesoporous Mat.*, 63 (2003) 125-137.
- [33] C. Lu, F. Su, S.-C. Hsu, W. Chen, H. Bai, J. F. Hwang, H.-H. Lee, *Fuel Process*. *Technol.*, 90 (2009) 1543-1549.
- [34] A. Samanta, A. Zhao, K. H. Shimizu, P. Sarkar, R. Gupta, *Ind. Eng. Chem. Res.*, 51 (2012) 1438-1463.
- [35] A. Corrias, G. Ennas, G. Mountjoy, G. Paschina, *Phys. Chem. Chem. Phys.*, 2 (2000) 1045-1050.
  - [36] K. Chayakul, T. Srithanratana, S. Hengrasmee, Catal. Today, 175 (2011) 420-429.
- [37] K. Chayakul, T. Srithanratana, S. Hengrasmee, *J. Mol. Catal. A: Chem.*, 340 (2011) 39-47.
  - [38] J.A. Rodriguez, Langmuir, 4 (1988) 1006.
  - [39] H.-J. Freund, M. W. Roberts, Surf. Sci. Rep. 25 (1996) 225-273.

# **OUTPUT OF THE RESEARCH**

#### M.SC. Student

1) Mr.Somkiat Krachuamram, (2013-2016): Synthesis and modification of zeolite X for carbon dioxide adsorption" Master of Science Thesis in Chemistry, Graduate School, Khon Kaen University.

#### **Publication papers**

- Somkiat Krachuamram, Chanaiporn Danvirutai, Sujittra Youngme, <u>Kingkaew Chayakul</u>
   <u>Chanapattharapol\*</u>, Effects of Cetyltrimethylammonium Bromide and Heptane on the
   Surface Properties and CO<sub>2</sub> Adsorption of Zeolite NaX, *Journal of the Chinese Chemical* Society 64 (2017) 658-665.
- Kingkaew Chayakul Chanapattharapol\*, Somkiat Krachuamram, Sujittra Youngme, Study of CO<sub>2</sub> adsorption on iron oxide doped MCM-41, *Microporous and Mesoporous Materials* 245 (2017) 8-15.

#### **Presentations**

- Somkait Krachuamram, Chanaiporn Danvirutai and Kingkaew Chayakul Chanapattharapol (2016). Synthesis and modification of mesoporous LTA zeolite for CO<sub>2</sub> adsorption.
   Poster presentation at Pure and Applied Chemistry International Conference 2016 (PACCON2016), BITEC, Bangkok, Thailand, 9-11 February 2016.
- Somkait Krachuamram, Chanaiporn Danvirutai and Kingkaew Chayakul Chanapattharapol (2016). The study of CO<sub>2</sub> adsorption on amine-modified mesoporous zeolite NaX.
   Poster presentation at International Congress for Innovation in Chemistry (PERCH-CIC Congress IX), Jomtien Palm Beach Hotel And Resort, Pattaty, Chonburi, Thailand. 26-29 June 2016.
- Somkait Krachuamram, Chanaiporn Danvirutai, Kingkaew Chayakul
   Chanapattharapol (2016). Synthesis of pore axpanded zeolite NaX and its CO<sub>2</sub>

**adsorption properties**. Poster presentation at The 3<sup>rd</sup> International Congress on Advanced Materials (AM 2016), Bangkok, Thailand 27-30 November 2016.

# **APPENDICES**

# Publication paper of part 1

Somkiat Krachuamram, Chanaiporn Danvirutai, Sujittra Youngme, <u>Kingkaew Chayakul Chanapattharapol\*</u>, Effects of Cetyltrimethylammonium Bromide and Heptane on the Surface Properties and CO<sub>2</sub> Adsorption of Zeolite NaX, *Journal of the Chinese Chemical Society* 64 (2017) 658-665. (IF 2016 = 0.935)

## Publication paper of part 2

 Kingkaew Chayakul Chanapattharapol\*, Somkiat Krachuamram, Sujittra Youngme, Study of CO<sub>2</sub> adsorption on iron oxide doped MCM-41, *Microporous and Mesoporous Materials* 245 (2017) 8-15. (IF 2016 = 3.615)